The Astrophysical Journal, 877:110 (16pp), 2019 June 1 https://doi.org/10.3847/1538-4357/ab1a41

SPIRITS Catalog of Infrared Variables: Identification of Extremely Luminous Long Period Variables

V. R. Karambelkar[1,2], S. M. Adams[1], P. A. Whitelock[3,4], M. M. Kasliwal[1], J. E. Jencson[1], M. L. Boyer[5], S. R. Goldman[5], F. Masci[6], A. M. Cody[7], J. Bally[8], H. E. Bond[5,9], R. D. Gehrz[10], M. Parthasarathy[11], and R. M. Lau[12]
(SPIRITS Collaboration)

[1] Cahill Center for Astrophysics, California Institute of Technology, Pasadena, CA 91125, USA; viraj.k@iitb.ac.in
[2] Department of Physics, Indian Institute of Technology Bombay, Mumbai 400076, India
[3] South African Astronomical Observatory, P.O. Box 9, 7935 Observatory, South Africa
[4] Department of Astronomy, University of Cape Town, Private Bag X3, Rondebosch 7701, South Africa
[5] STScI, 3700 San Martin Drive, Baltimore, MD 21218, USA
[6] Infrared Processing and Analysis Center, California Institute of Technology, Pasadena, CA 91125, USA
[7] NASA Ames Research Center, Moffett Field, CA 94035, USA
[8] Center for Astrophysics and Space Astronomy, University of Colorado, UCB 389 Boulder, CO 80309, USA
[9] Department of Astronomy and Astrophysics, Pennsylvania State University, University Park, PA 16802, USA
[10] Minnesota Institute for Astrophysics, 116 Church Street S. E., Minneapolis, MN 55455, USA
[11] Indian Institute of Astrophysics, Koramangala, Bangalore 560034, India
[12] Institute of Space & Astronautical Science, Japan Aerospace Exploration Agency, Sagamihara, Kanagawa 252-5210, Japan
Received 2019 January 22; revised 2019 March 26; accepted 2019 April 9; published 2019 May 31

Abstract

We present a catalog of 417 luminous infrared variable stars with periods exceeding 250 days. These were identified in 20 nearby galaxies by the ongoing SPitzer InfraRed Intensive Transients Survey survey with the *Spitzer Space Telescope*. Of these, 359 variables have $M_{[4.5]}$ (phase-weighted mean magnitudes) fainter than −12 and periods and luminosities consistent with previously reported variables in the Large Magellanic Cloud (LMC). However, 58 variables are more luminous than $M_{[4.5]} = -12$, including 11 that are brighter than $M_{[4.5]} = -13$, with the brightest having $M_{[4.5]} = -15.51$. Most of these bright variable sources have quasi-periods longer than 1000 days, including four over 2000 days. We suggest that the fundamental period–luminosity relationship, previously measured for the LMC, extends to much higher luminosities and longer periods in this large galaxy sample. We posit that these variables include massive asymptotic giant branch (AGB) stars (possibly super-AGB stars), red supergiants experiencing exceptionally high mass-loss rates, and interacting binaries. We also present 3.6, 4.5, 5.8, and 8.0 μm photometric catalogs for all sources in these 20 galaxies.

Key words: stars: AGB and post-AGB – stars: oscillations (including pulsations)

Supporting material: machine-readable table

1. Introduction

The parameter space of stellar optical variability has been explored for centuries, revealing many classes of variable stars (see, e.g., Gaia Collaboration et al. 2019, for a review). However, significant (>0.3 mag) variability with long periods (>200 days) in luminous (brighter than $M_{\rm bol} = -4$) stars is primarily limited to luminous blue variables (LBVs), pulsating red supergiants (RSGs), and asymptotic giant branch (AGB) stars (Samus et al. 2017). These three classes of long-period variables (LPVs), which have periods longer than a few hundreds of days, can be prolific dust producers and require observations in the infrared (IR) to understand their spectral energy distributions and dust production. But until recently, there have been few IR variability surveys with sufficiently long temporal baselines.

AGB stars constitute a large proportion of long-period IR variables and the largest amplitudes are found among the Mira variables, which tend to be at the tip of the AGB (Soszyński et al. 2009; Whitelock et al. 2017). These variables have been studied by various surveys of the Local Group. Working in the near-IR (*JHK*(*L*)), Feast et al. (1989) and Hughes & Wood (1990) discovered and studied numerous LPVs in the Large Magellanic Cloud (LMC). This has gradually been extended to other Local Group galaxies (e.g., Menzies et al. 2015; Whitelock et al. 2018, and references therein). The Optical Gravitational Lensing Experiment (Udalski et al. 1993) has also characterized large numbers of LPVs in the Magellanic Clouds and elsewhere (e.g., Soszyński et al. 2009), with sufficient data to derive excellent periods. Recently, Ita et al. (2018) presented *JHK* time series data for the central region of the Small Magellanic Cloud (SMC).

Using 8 bands of IR photometric data from the Surveying the Agents of Galaxy Evolution (Meixner et al. 2006) survey and periods from the Massive Compact Halo Object (Alcock et al. 1993) survey, Riebel et al. (2010) reported the IR period–luminosity (PL) relations for around 30,000 AGB stars in the LMC. Riebel et al. (2015) employed the variability criteria described in Vijh et al. (2009) to identify variables in the LMC and SMC using 3.6 and 4.5 μm data. They found 10 new dust-obscured large-amplitude AGBs in the LMC and six in the SMC. These objects are not detected by optical surveys, and hence do not have a measured optical variability. Dust in Nearby Galaxies with *Spitzer* (DUSTiNGS; Boyer et al. 2015) is a 3.6 and 4.5 μm survey of 50 dwarf galaxies to identify dust producing AGB stars. Using two epochs and the variability

criteria defined by Vijh et al. (2009), this survey identified 710 variables in these galaxies.

AGB stars can be classified into carbon-rich and oxygen-rich variables based on their surface C/O-ratios. This can be done using spectroscopy or narrow-band photometry. AGB stars with the reddest [3.6]–[4.5] colors are considered "extreme" AGB stars (eAGB; Thompson et al. 2009; Boyer et al. 2015). While this is a normal phase of stellar evolution, eAGBs are characterized by the extreme amounts of dust enshrouding them, and are a major contributor to the dust content of the ISM (Matsuura et al. 2009; Riebel et al. 2012).

AGB stars can also be classified based on their periods. The periods of large-amplitude AGB variables are typically longer than 100 days. These stars can oscillate in their fundamental modes (as do Miras) or exhibit overtones. The fundamental modes have periods ranging from 100 to 1000 days, while the overtones are characterized by shorter periods. AGB variables exhibit a linear log(period)–log(luminosity) relationship. The different modes of oscillation can be separated into six sequences in the period–luminosity space (Wood et al. 1999). Menzies et al. (2019) recently summarized what is known about Miras with periods longer than 1000 days. There are only 17 known in the Galaxy, 18 in the LMC, and 3 in the SMC. The longest period (1859 days) is for MSX-SMC-055, which is discussed in Section 3.

Super-AGB stars are a subclass of AGB stars at the upper end of the AGB mass range (8–12 $M_{\odot}$). These stars are expected to evolve similarly to the slightly less massive oxygen-rich AGB stars, but ultimately explode as electron-capture supernovae or produce ONe white dwarfs. Super-AGB stars are also expected to pulsate, populating the high-luminosity end of the AGB period–luminosity relationship for fundamental mode pulsators. While super-AGB stars have a strong theoretical backing (Siess 2007; Doherty et al. 2015, 2017), it has been difficult to identify them observationally. Their observed properties tend to be very similar to red supergiants and other massive AGB stars, and they are also expected to be quite rare. The IR pulsation properties provide an additional clue toward confidently identifying these objects. The amplitudes of variability of these super-AGB stars are expected to be larger than those of RSGs, and may be a key for distinguishing between the two. We discuss the AGB stars in our sample in Section 3.2 and the potential super-AGBs in Section 3.3.

Dusty oxygen-rich AGB and RSG stars in their final evolutionary stages exhibit circumstellar OH maser emission. These stars are obscured in the optical, but bright in the IR due to the large quantity of dust surrounding them. These stars are designated as OH/IR stars. The OH maser emission is strongest at 1612 MHz. Goldman et al. (2017, 2018) identified OH/IR stars in the LMC and SMC, and reported their periods and among other photometric data, their *Spitzer* (Werner et al. 2004; Gehrz et al. 2007) InfraRed Array Camera (IRAC; Fazio et al. 2004) 3.6 and 4.5 μm magnitudes. Whitelock et al. (2017) and Boyer et al. (2015) noted correlations, with more luminous stars being dustier (redder [3.6]–[4.5] colors) and dustier stars having larger amplitudes in the IR variability. The evolution of binary stars (e.g., De Marco & Izzard 2017) can also give rise to both variability and mass loss. It seems possible that massive stars in wide binaries, such as η Carinae, and common-envelope stars, such as Thorne–Żytkow Objects (TZOs) will be among our sources. This is discussed briefly in Section 3.3.

Until recently, the largest IR variability surveys using *Spitzer* were limited to the LMC and SMC (Vijh et al. 2009; Riebel et al. 2015), M33 (McQuinn et al. 2007), and nearby dwarf galaxies with DUSTiNGS (Boyer et al. 2015). These surveys are limited to lower-mass galaxies and/or are comprised of a small number of epochs over a small time baseline (requiring the use of variability indices and periods from near-IR/optical surveys). Accordingly, these surveys do not provide a complete census of the most dusty and obscured IR variables.

Since 2014, the SPitzer InfraRed Intensive Transients Survey (SPIRITS; Kasliwal et al. 2017) has been monitoring nearly 200 nearby ($d < 30$ Mpc) galaxies (typically with cadences of 3–6 months) using *Spitzer*/IRAC to (primarily) search for IR transients. A detailed description of the galaxy sample, depth, and cadence of observations of the SPIRITS survey can be found in Kasliwal et al. (2017). In this paper we present the IR variable stars identified in the closest and most luminous galaxies in the SPIRITS survey. In Section 2 we describe our galaxy sample, source catalogs, photometry, period-fitting, and variable classification. In Section 3 we present our results and suggest that the period–IR luminosity relation measured in the LMC and SMC extends to longer periods and higher luminosities than previously observed. This relation extends beyond the maximum luminosity expected for AGB stars, suggesting that the most luminous IR variables in our sample may be pulsating super-AGB stars or RSGs experiencing exceptionally high mass-loss rates.

2. Catalog Construction

2.1. Galaxy Sample

In this paper, we generate point-spread function (PSF) catalogs and identify variables in the closest and most luminous galaxies in the SPIRITS survey using a two-tiered selection strategy that includes the 9 galaxies within 1 Mpc targeted by SPIRITS in addition to the 11 galaxies within 10 Mpc targeted by SPIRITS with *B*-band absolute magnitudes brighter than −20.6. Beyond 10 Mpc, accurate stellar photometry of all but the most luminous stars becomes extremely difficult. Our two-tiered strategy allows for adequate coverage of both: the more common lower-luminosity AGBs (that belong to the nearby galaxies), as well as the rare high-luminosity variables (that belong predominantly to the distant galaxies). It also enables us to validate our methodology against existing works. Our galaxy sample includes four nearby dwarf galaxies that were targeted by the DUSTiNGS survey. In Section 3.1 we compare our analysis of variables in the four DUSTiNGS galaxies to that by S. R. Goldman et al. (2019, in preparation). Table 1 lists the galaxies in our sample and summarizes their properties.

2.2. Reference Photometry

Following the approach of Kasliwal et al. (2017) we adopt the [3.6], [4.5], [5.8], and [8.0] supermosaic images of each galaxy from the Spitzer Heritage Archive[13] as reference images. We used the DAOPHOT/ALLSTAR (Stetson 1987) package to perform PSF photometry on these images. For each reference image, the PSF was constructed using isolated stars in the image. A 2.″4 disk was used to measure the brightness of sources and an annulus of 2.″4–7.″2 was used to estimate sky background while constructing the PSF. We used a PSF fitting

[13] http://sha.ipac.caltech.edu/

Table 1
Galaxy Properties

Galaxy	Number of SPIRITS Sources	Number of Variables		Distance (Mpc)	Number of Epochs	Stellar Mass ($M_\odot$)	B mag (mag)	SFR $\log(M_\odot \mathrm{yr}^{-1})$
		Total	Bright[a]					
Fornax	21	0		0.15	12	2.0×10^7	−11.5	
Leo I	50	1		0.26	12	5.5×10^6	−11	
NGC 6822	200	35		0.48	28	1.66×10^9	−15.2	−1.9
NGC 185[b]	126	56		0.63	16	1.38×10^8	−14.7	−4.73
NGC 147[b]	57	18		0.73	13	6.2×10^7	−14.8	−6.33
M32[c]	171	0		0.78	9	3.2×10^8	−14.8	−5.88
IC 1613[b]	61	10		0.74	28	7.6×10^7	−14.5	−2.35
M110	389	189		0.81	14	1.91×10^8	−16.1	<-7.73
WLM[b]	51	12		0.96	24	1.86×10^8	−14.1	−2.68
IC 342	216	10	3	3.39	15	1.41×10^{11}	−20.7	−0.26
M81	64	16	5	3.61	37	1.86×10^{11}	−20.9	0
M83	130	52	33	4.66	26	2.09×10^{11}	−20.6	0.44
NGC 6946	29	2	1	5.89	38	7.76×10^{10}	−20.8	0.63
M101	37	12	12	6.95	33	2.24×10^{11}	−21.1	0.46
M106	2	1	1	7.31	15	2.14×10^{11}	−21.2	0.44
M51	22	1	1	8.58	34	4.17×10^{10}	−21.4	0.46
NGC 6744	5	2	2	8.95	16	2.24×10^{11}	−21	0.35
M63	13	0		8.95	16	2.19×10^{11}	−21	0.21
NGC 2903	13	0		9.33	15	1.35×10^{11}	−20.9	−2.93
M104	8	0		10.22	16	5.75×10^{11}	−21.8	−1

Notes. The stellar masses, B-band magnitudes, and integral star formation rates (SFRs) are from Karachentsev et al. (2013). The distances are taken from the Cosmicflows-3 catalog (Tully et al. 2017), with the exception of NGC 6946, where the distance is from the Karachentsev et al. (2013) catalog because it does not have a Cosmicflow-3 distance.

[a] The bright variables are those with $M_{[4.5]}$ brighter than −12 (which is close to the maximum luminosity of the LMC AGB sample examined by Riebel et al. 2010).

[b] Indicates galaxies that are also included in the DUSTiNGS survey (NGC 185, NGC 147, IC 1613 and WLM).

[c] We exclude the variables detected in M32, because the number of epochs for this galaxy is smaller than 10.

radius of 4.″2, which is roughly 2.5 times the FWHM of the PSF.

As the PSF was terminated at a finite radius and not allowed to extend to infinity, there is a slight underestimation of the total flux. To correct for this, we followed the procedure described in Khan et al. (2015). We performed aperture photometry on all sources in our PSF catalog for each image, using IRAF ApPhot/Phot. We used an aperture radius of 2.″4 with a sky annulus of 2.″4–7.″2, and empirically derived aperture corrections of 1.213, 1.234, 1.379, and 1.584 for the 3.6, 4.5, 5.8, and 8.0 μm channels, respectively. The difference between aperture and PSF magnitudes of a source is an indication of crowding of stars around that source. The sources for which this difference is relatively small are relatively isolated in the image. We calculated the mean of the difference between PSF and aperture magnitudes for these relatively isolated sources for each image, and used it as a zero-point offset to account for the flux underestimation due to finite PSF fitting radius. Following Khan et al. (2015), we perform this correction procedure for all but the 8.0 μm images, which are badly affected by crowding.

We identified all sources that are $>1\sigma$ brighter than the background and have PSF magnitude uncertainties smaller than 0.3. The instrument magnitudes were converted to apparent magnitudes using the Vega-calibrated zero-points of 18.80, 18.32, 17.83, and 17.20 for the 3.6, 4.5, 5.8, and 8.0 μm channels, respectively.[14]

[14] http://irsa.ipac.caltech.edu/data/SPITZER/docs/dataanalysistools/

The 3.6, 4.5, 5.8, and 8.0 μm photometric catalogs for all sources in the 20 galaxies are available in Zenodo at doi:10.5281/zenodo.2643483. We present the number of sources in each of the catalogs in Table 2. Khan et al. (2015) and Khan (2017) presented PSF catalogs for 22 SPIRITS galaxies (including seven of the galaxies we consider in this paper). We validate our procedure for constructing PSF catalogs by comparing our 3.6 and 4.5 μm catalogs for the galaxies NGC 2903, M83, NGC 6822, NGC 6946, M51, M101, and M81 to those of Khan (2017) using a matching radius of 1″. The average magnitude difference between the two catalogs for each galaxy and filter combination is less than 0.05. In Figure 1, we plot the $M_{[4.5]}$ magnitudes versus [3.6]–[4.5] colors for all the sources in our catalogs for each galaxy. We also highlight the positions in the color–magnitude diagrams of the variables we present in Section 3. Most of these variables have [3.6]–[4.5] > 0.

It is possible that the magnitudes of the brightest sources are inflated due to biases in the photometric procedure. To check for this, we performed an artificial star test on M101: the most distant and luminous galaxy in the sample that contains many of these bright variables. We used the derived PSFs to inject 1000 artificial stars with magnitudes ranging from 10 to 20 uniformly distributed into the 3.6, 4.5, 5.8 and 8.0 μm images of this galaxy. We perform the procedure described above to extract the magnitudes of these stars. We repeat this procedure 10 times and plot the behavior of injected−recovered magnitudes for the 50th and 90th percentile of recovered sources in Figure 2. At $M_{[4.5]} = -13$ for this galaxy, 90% of

Table 2
PSF Catalog Properties[a]

Galaxy	[3.6]	[4.5]	[5.8]	[8.0]
Fornax	48804	49868	17613	16777
Leo I	44766	43634	196[b]	63402
NGC 6822	52262	55686	101348	113344
NGC 185[a]	14659	14165	11625	13440
NGC 147[a]	13307	12813	13629	13013
M32	25818	28188	160818	212120
IC 1613[a]	18006	21093	24176	20842
M110	41156	40606	205870	205209
WLM[a]	13169	16514	19284	20465
M104	35462	36667	54715	62910
M51	33829	36326	87755	93462
M106	23874	31840	28739	75601
M101	46770	46431	124846	199673
NGC 6744	16397	17089	11294	20103
M63	41888	45237	112676	121404
M81	44023	42785	228825	242552
NGC 2903	58593	66706	94257	95640
NGC 6946	37219	38389	94773	89262
IC 342	115573	123278	163581	141576
M83	55682	57117	400578	304464

Notes.
[a] Number of sources in the catalogs for each channel.
[b] The 5.8 μm reference image for Leo I is shallow, resulting in a low number of sources.

recovered sources have a bias less than 0.15 mag. For the closer galaxies the bias should be even smaller, implying that our brightest variables do not suffer from large photometric biases.

2.3. Variable Source Identification and Photometry

We utilize the list of variable sources identified from the image subtraction pipeline and visually vetted as described in Kasliwal et al. (2017). In an effort to minimize contamination of the photometry from image subtraction artifacts and nearby variable sources, we use the smaller aperture sizes described in Section 2.2 to generate difference photometry (rather than the larger aperture sizes given in Kasliwal et al. 2017).

The statistical uncertainties in the difference imaging photometry are much smaller than the true uncertainties arising from artifacts and other systematics. To more accurately reflect these uncertainties, for each epoch we add (in quadrature) the rms of the reference-subtracted photometry of a grid of points within 7.″2 of the target to the statistical uncertainty.

We cross-match the sources flagged by the SPIRITS pipeline to 3.6 and 4.5 μm reference catalogs using a matching radius of 1″ and retain the closest matching source. The number of sources for each galaxy is given in Table 2.

2.4. Period Fitting

We simultaneously fit the 3.6 and 4.5 μm light curves of all cross-matched sources with the GATSPY (VanderPlas & Ivezić 2015; Vanderplas 2015) implementation of the Lomb–Scargle method (Lomb 1976; Scargle 1982). Given the relatively sparse light-curve sampling we restrict our periodicity search to sinusoidal signals. We create an initial list of likely variables from the light curves that meet all of the following selection criteria:

1. Null χ^2–reduced $\chi^2 > 3$, where null χ^2 is the reduced χ^2 for constant flux.
   (a) Ensures the periodic model is a significant improvement over a model with constant flux.
2. Best-fit period $<0.8\times$ light-curve duration and best-fit period $<$ light-curve duration -50 days.
   (a) With poorly sampled data periods $\gtrsim$ the light-curve durations are unreliable.
3. Best-fit period >250 days.
   (a) Periods must be significantly longer than typical cadences in order to avoid aliasing.
4. Best Lomb–Scargle score >0.8.
5. (Best Lomb–Scargle score)/(Second-best Lomb–Scargle score) > 1.06.
   (a) Requiring the highest peak in the periodogram to be significantly higher than the 2nd highest peak eliminates many sources plagued by aliasing or poor fits.
6. Number of epochs of observation greater than 10.

We calculate phase-weighted mean magnitudes and peak-to-peak amplitudes for all the sources that meet these selection criteria.

The number of observations and cadence varies between galaxies and between individual variables. Thus, our confidence in the periods and amplitudes listed depends strongly on the details of the observations of the individual sources. We therefore aimed to assign a (subjective) quality to each variable identified that is based on visual inspection of the light curves and periodograms as follows: gold: very likely to be a periodic variable; silver: a possible periodic or quasi-periodic variable; bronze: not, or unlikely to be, periodic. However, given the large sample size of our sources, it is not feasible to do this for all variables. Hence, we limit this exercise only to the sources with $M_{[4.5]}$ brighter than -12, as these are brighter than the most luminous LMC AGB variables examined by Riebel et al. (2010) and constitute the most interesting variables in our sample. Some of the interesting variables in the bronze classification are briefly described in the Appendix. At this point, we would like to draw attention to the fact that the process of identifying transients and variables involved members of the SPIRITS collaboration examining each new set of observations. These were presented to them as image subtractions, using earlier 3.6 and 4.5 μm images as references. Individuals would identify "sources" as those of interest or junk. Depending on various factors, including the density of earlier observations, the cadence, and the timing of the transient, some confusion between categories was inevitable. Some of the most interesting variables are in very crowded star-forming regions, so isolating them is a challenge. Added to this is the fact that the cadence and the total number of observations are often not ideal for characterizing LPVs. Altogether, these factors make the survey incomplete and in many cases we cannot definitively distinguish between periodicity and quasi-periodicity. In addition, crowding and limited sensitivity of IRAC to the distant galaxies in our sample are likely to inflate the magnitudes reported here by a small amount. Nevertheless, the results indicate the existence of a tantalizing population of large-amplitude infrared luminous sources with a range of properties, as discussed below.

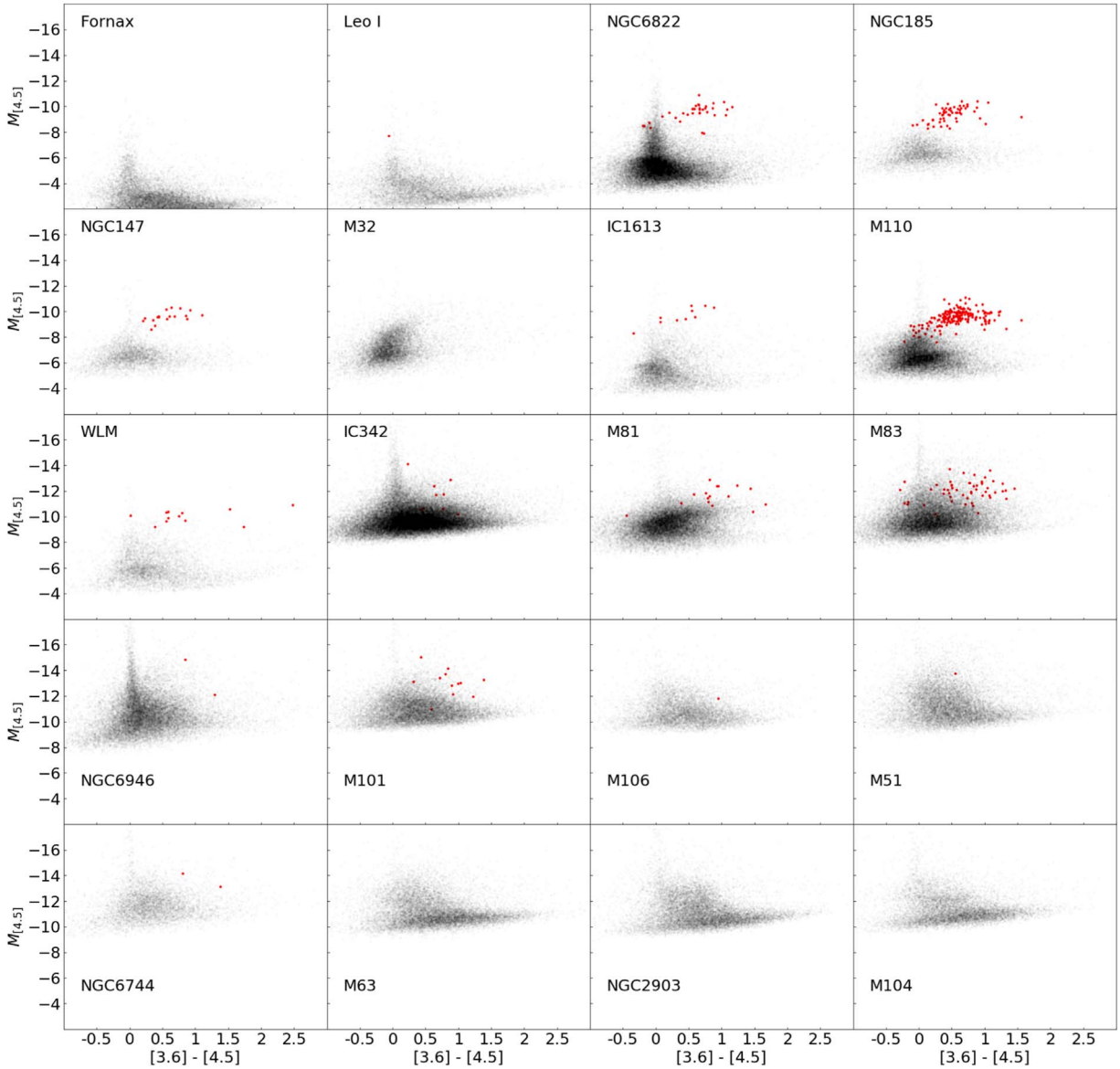

Figure 1. Reference $M_{[4.5]}$ vs. [3.6]–[4.5] colors for our variables in each galaxy (red dots in each panel), with the $M_{[4.5]}$ vs. [3.6]–[4.5] for the entire galaxy as the background (small black points). To generate the background, we cross-match the 3.6 μm catalogs with our 4.5 μm catalogs, using a radius of 1″. We find that most of our variables are among the reddest objects in the galaxies. It is also evident that the reddest variables are generally at the top of the luminosity distribution.

3. Results

We identify 417 candidate luminous LPVs in the galaxies in our sample and present their periods and phase-weighted mean absolute magnitudes, $M_{[3.6]}$ and $M_{[4.5]}$, in Table 3. We cross-match these variables to the reference 5.8 and 8.0 μm images using a matching radius of 1″ and retain the closest matching source and find matches in both the 5.8 and 8.0 μm reference images for 160 of these variables.

In the following we discuss possible origins of the variability of these SPIRITS sources in terms of pulsation (AGB variables), via interacting dusty winds in binary systems (WRC stars) or via orbital modulation, also in binaries. Other causes may contribute, e.g., eruptive variability, particularly if very long term monitoring suggests the variations are only quasi-periodic, e.g., LBVs.

We plot the period–luminosity relation for the sources in our sample using the derived periods and their phase-weighted mean magnitudes in Figure 3. The sequences corresponding to the fundamental and first overtone modes of evolved variables in the LMC (Riebel et al. 2010) are populated in the diagram. The variables in the nearby galaxies in our sample closely match luminosities and periods of the LMC variables (for periods longer than our 250 days threshold and absolute magnitudes brighter than −8). Along with these, we also find variables that are more luminous and have longer periods than the LMC variables and lie in a previously largely empty region of the period–luminosity diagram. We note that there is a scarcity of variables with periods between 650–1200 days, and $M_{[4.5]}$ between −11 and −12. This gap is most likely a product of our limited sensitivity, and we discuss it in Section 3.2.

In Figure 4, we plot the SPIRITS variables color-coded by their peak-to-peak amplitudes of variability. We note that a majority of our lower-luminosity sources have relatively low amplitudes, from 0.5 to 1. The higher-amplitude sources are predominantly found at higher luminosities and longer periods

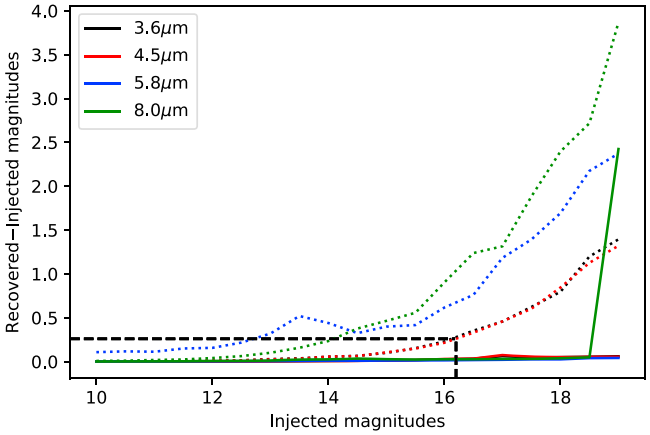

Figure 2. Artificial star test results for M101. The dotted lines indicate the behavior of the 90th percentile of recovered sources and the solid lines indicate the behavior of the 50th percentile of recovered sources. At $M_{[4.5]} = -13$ (marked in black dashed lines) for this galaxy, 90% of recovered sources have a bias less than 0.25. For the closer galaxies the bias should be even smaller, implying that our brightest variables do not suffer from large photometric biases.

and in particular within the group that is probably high-mass AGB stars (see Section 3.3).

We also plot the $M_{[4.5]}$ versus [3.6]–[4.5] color–magnitude diagram of the SPIRITS variables in Figure 5, color-coded by their period. Overplotted are the variables from the LMC reported by Riebel et al. (2015). We find a large group of variables with periods in the range of 250–750 days, which coincides with the AGB region of the LMC. The longer-period variables are more luminous than these and have colors between −0.5 and 1.5. Also marked in the color–magnitude diagram is the region identified by Thompson et al. (2009) ($M_{[4.5]} < -10$ and [3.6]–[4.5] > 1.5 mag) containing progenitors of SN2008S-like events. We also plot the $M_{[8.0]}$ versus [3.6]–[8.0] color–magnitude (Figure 6) and [3.6]–[4.5] versus [5.8]–[8.0] color–color (Figure 7) diagrams for the sources that find matches in the 5.8 and 8.0 μm reference images. We note that in Figure 6, our AGB candidates exhibit a sequence, while the luminous ($M_{[4.5]}$ brighter than −12) candidates lie on a different, more luminous sequence. In the color−color diagram (Figure 7), we also plot the expectation for a blackbody at temperatures of 5000, 1000, 500, and 350 K. The diagram suggests that the long-period sources in our sample are extremely cold and have an IR excess due to large amounts of dust enshrouding them. However, most of the luminous sources belong to clusters or are near H II regions. This, coupled with the fact that the PSF is large at 8.0 μm, could inflate the brightness and colors of these sources.

3.1. Comparison of SPIRITS and DUSTiNGS

In this section we compare our variable catalog with the four galaxies in the DUSTiNGS survey recently analyzed by S. R. Goldman et al. (2019, in preparation). The DUSTiNGS survey identifies 62 AGB candidates in the four galaxies we have in common (NGC 147, NGC 185, IC 1613, and WLM), while we identify 95 variables in these galaxies. The SPIRITS and DUSTiNGS lists have 25 sources in common. It is possible that some of the DUSTiNGS variables were missed by SPIRITS during the process of human scanning (see Section 2.4). Figures 8–10 compare our periods, [3.6] absolute mean magnitudes, and [3.6] amplitudes with corresponding DUSTiNGS values for these 25 variables. The SPIRITS periods and magnitudes agree well with the DUSTiNGS values, with an average scatter of 9 days and 0.1 mag, respectively, while the amplitudes have a slightly larger scatter of 0.13.

3.2. AGB Candidates

We identify 359 variables in our sample with 4.5 μm mean absolute magnitudes fainter than −12 (which is close to the maximum luminosity of the LMC AGB sample examined by Riebel et al. 2010). Nearly all of these lie along the known period–luminosity relation for AGBs. These sources predominantly belong to the nearby dwarf galaxies and are most likely pulsating AGB stars from these galaxies. Like the LMC variables, most of the sources in our sample also fall where we would expect for the fundamental or first overtone pulsators in the period–luminosity diagram. However, as mentioned in Section 2.4, we do not visually inspect the light curves of these candidates. Thus, it is possible that some of these sources do not have well defined periods.

Most of these variables have periods around 250–750 days, while a handful of them are oscillating with longer periods around and larger than 1000 days. The fundamental pulsators have absolute magnitudes between −8 and −11. As a representative of this group, we present the phase-folded light curve of SPIRITS 14va (Figure 11) in the galaxy WLM, with a period of 511 days and a mean 4.5 μm magnitude of −10.26.

The longest period variables with $M_{[4.5]} > -12$ have periods ranging from 1400 up to 3200 days. SPIRITS 15acg (Figure 12) in NGC 185 belongs to this category, with a period of 1407 days, as do SPIRITS 14ct (Figure 13) in NGC 6822, with a period of 2947 days, and SPIRITS 15aci (Figure 14) in NGC 185. Some of these are known C-stars, which possibly have long secondary periods or erratic variations; SPIRITS 14bjc (Letarte et al. 2002) in NGC 6822 and SPIRITS 15aci (Nowotny et al. 2003) are examples of this type. Other variables are almost certainly quasars (or other active galactic nuclei); SPIRITS 14ary ($M_{[4.5]} = -10.34$ period = 1806 days), nominally in IC 1613, would be one example of these (Flesch 2017).

In the $M_{[4.5]}$ versus [3.6]–[4.5] color–magnitude diagram (Figure 5), the AGB candidates having $M_{[4.5]}$ fainter than −11 form a group and trace the AGB of the LMC variables color–magnitude diagram. The brighter AGB candidates in this sample show more scatter, but there are no significant deviations from the trends exhibited by the LMC AGB variables. The three long-period candidates (>2000 days) have [3.6]–[4.5] < 0.5 and occupy the same region as shorter-period AGB candidates, supporting the idea that the long periods found from the Spitzer data may be secondary.

The reddest and brightest sources among these are referred to as extreme AGB (eAGB) variables. Thompson et al. (2009) identify eAGB stars in M33, and look for progenitors of SN2008S and NGC 300-like transients in these galaxies. They note the reasonable criteria for eAGB stars to be identified as analogs of progenitors of these transients are $M_{[4.5]} < -10$, [3.6]–[4.5] > 1.5, and small amplitude variability (amplitude < 0.3 mag). There are four periodic variables in this extremely red region of the CMD, but all have amplitudes larger than 0.9 mag.

There is a tantalizing paucity of stars on the extrapolated PL relation with periods between 650 and 1200 days. However, this

Table 3
Variable Catalog

Name	R.A.	Decl.	Gal	Period	$M_{[3.6]}$	$M_{[4.5]}$	Δ[3.6]	Δ[4.5]	Quality	References
14apu	210.882379	54.373631	M101	1752	−14.93 ± 0.06	−15.51 ± 0.03	0.29	0.25	silver	1
14aue	56.70243	68.067607	IC342	344	−14.31 ± 0.03	−14.80 ± 0.03	0.14	0.11	gold	2
15ty	308.730675	60.135467	N6946	1587	−13.97 ± 0.04	−14.80 ± 0.06	0.47	0.43	gold	2, 3, 4
15pk	210.885626	54.295308	M101	1750	−13.38 ± 0.03	−14.20 ± 0.07	0.24	0.29	bronze	1
18ec	202.512772	47.170201	M51a	2538	−13.42 ± 0.08	−13.97 ± 0.07	0.54	0.60	gold	5
14axv	287.472939	−63.823283	N6744	381	−12.82 ± 0.07	−13.62 ± 0.08	1.75	1.88	bronze	SN2005at
15js	204.211515	−29.873467	M83	1603	−12.87 ± 0.03	−13.59 ± 0.03	0.95	0.86	silver	6
14apz	210.718431	54.336889	M101	1397	−12.00 ± 0.12	−13.48 ± 0.04	1.52	0.99	gold	1, 2
16do	204.279883	−29.89054	M83	2071	−12.35 ± 0.07	−13.47 ± 0.04	0.36	0.42	silver	
15jt	204.284774	−29.848441	M83	928	−13.00 ± 0.11	−13.42 ± 0.19	0.53	0.76	silver	8
16po	204.256266	−29.907444	M83	1206	−12.56 ± 0.03	−13.35 ± 0.05	0.39	0.32	bronze	9
14aq	149.082516	69.06756	M81	824	−12.17 ± 0.02	−12.97 ± 0.03	0.61	0.23	bronze	
14apy	210.718747	54.297112	M101	1679	−12.21 ± 0.06	−12.94 ± 0.09	1.16	1.56	silver	1
14aqa	210.803966	54.362223	M101	1682	−11.16 ± 0.11	−12.94 ± 0.05	1.56	0.92	bronze	1, 10
15agi	56.505276	68.092698	IC342	929	−12.09 ± 0.07	−12.93 ± 0.07	0.45	0.51	gold	
14bpf	204.27225	−29.883631	M83	1234	−11.92 ± 0.04	−12.89 ± 0.08	0.82	0.88	gold	
16pn	204.292494	−29.879432	M83	1158	−11.91 ± 0.04	−12.84 ± 0.04	0.60	0.64	silver	
15zg	204.269869	−29.843227	M83	1127	−11.87 ± 0.05	−12.77 ± 0.04	0.63	0.79	gold	7, 9, 11
15ke	204.258726	−29.879923	M83	857	−12.86 ± 0.06	−12.73 ± 0.04	0.29	0.45	gold	8, 12
14bot	204.170951	−29.874657	M83	1666	−12.60 ± 0.11	−12.65 ± 0.04	0.44	1.11	gold	
15kz	210.954843	54.369441	M101	1496	−11.55 ± 0.07	−12.62 ± 0.06	1.29	1.22	silver	1
15oe	287.456721	−63.819975	N6744	2372	−11.17 ± 0.10	−12.58 ± 0.04	3.40	2.47	silver	
14aul	56.533417	68.105675	IC 342	997	−11.90 ± 0.04	−12.57 ± 0.05	0.62	0.68	gold	
15jw	204.221199	−29.875165	M83	1787	−12.06 ± 0.07	−12.57 ± 0.07	0.65	1.05	gold	8, 12, 13
14akr	204.224543	−29.864975	M83	1964	−11.73 ± 0.06	−12.54 ± 0.07	1.22	1.06	silver	
15ky	210.75046	54.381013	M101	897	−12.35 ± 0.04	−12.51 ± 0.06	0.53	0.83	gold	1
16dp	204.24353	−29.896648	M83	1215	−12.06 ± 0.06	−12.50 ± 0.08	0.64	0.81	gold	
14bco	210.727875	54.288666	M101	1411	−11.71 ± 0.03	−12.50 ± 0.04	1.63	1.08	silver	
14akl	204.183788	−29.823974	M83	1506	−11.88 ± 0.01	−12.49 ± 0.02	0.88	0.80	silver	
15kd	204.235358	−29.871858	M83	1033	−11.78 ± 0.06	−12.48 ± 0.06	1.26	1.21	silver	
14ajs	204.311239	−29.834511	M83	1472	−11.25 ± 0.07	−12.46 ± 0.05	2.46	1.35	silver	
18ae	210.824216	54.314684	M101	1530	−11.24 ± 0.07	−12.45 ± 0.05	5.23	1.78	gold	2
15kc	204.20733	−29.838336	M83	1065	−11.99 ± 0.03	−12.43 ± 0.03	0.75	0.45	gold	12, 13
14bqb	204.253607	−29.917184	M83	1673	−11.67 ± 0.07	−12.42 ± 0.04	1.54	1.30	bronze	6, 9, 14
14apq	148.775969	69.127891	M81	1606	−11.68 ± 0.05	−12.40 ± 0.02	1.96	1.60	silver	
14atg	204.204003	−29.887841	M83	772	−12.00 ± 0.03	−12.40 ± 0.03	0.86	1.20	silver	15
15zh	204.296821	−29.863899	M83	1731	−11.27 ± 0.03	−12.33 ± 0.02	3.17	2.62	silver	
17fo	184.709724	47.303198	M106	1542	−11.16 ± 0.09	−12.30 ± 0.04	2.04	1.67	gold	
14bov	204.296388	−29.867147	M83	1656	−11.27 ± 0.03	−12.29 ± 0.02	1.08	1.29	silver	
14boy	204.246034	−29.811423	M83	1440	−11.06 ± 0.08	−12.29 ± 0.09	1.37	0.87	silver	
15km	204.241521	−29.843867	M83	1362	−11.80 ± 0.06	−12.28 ± 0.08	0.68	0.77	gold	
14bcp	210.748934	54.295433	M101	1592	−11.61 ± 0.05	−12.27 ± 0.08	0.85	1.32	gold	1
17kh	204.298281	−29.828349	M83	1218	−11.53 ± 0.08	−12.25 ± 0.08	0.79	0.58	gold	
14akp	204.274805	−29.94043	M83	1507	−11.41 ± 0.06	−12.23 ± 0.03	1.44	1.48	silver	
14ck	148.942537	68.995879	M81	1610	−11.13 ± 0.06	−12.22 ± 0.04	2.00	1.53	gold	
14oj	148.726763	69.068093	M81	2956	−10.82 ± 0.06	−12.22 ± 0.06	0.50	0.62	bronze	2
14akn	204.270461	−29.908382	M83	1430	−11.53 ± 0.05	−12.16 ± 0.04	1.02	1.20	silver	4, 9, 14
16dt	204.275987	−29.88318	M83	1089	−11.08 ± 0.05	−12.16 ± 0.03	1.08	0.80	gold	16
14ajf	210.844714	54.282388	M101	1527	−11.27 ± 0.07	−12.16 ± 0.12	1.22	1.42	gold	1
16ds	204.254718	−29.912643	M83	1377	−11.43 ± 0.05	−12.10 ± 0.04	0.72	0.94	silver	9, 14
15 mn	210.955989	54.347408	M101	1661	−10.66 ± 0.04	−12.10 ± 0.03	2.33	1.48	silver	1
15kj	204.215737	−29.849034	M83	1450	−11.64 ± 0.04	−12.08 ± 0.04	0.84	1.30	silver	
15ki	204.189008	−29.85111	M83	1119	−11.41 ± 0.04	−12.05 ± 0.03	1.06	0.92	gold	2, 13
14aks	204.206609	−29.79767	M83	1426	−11.14 ± 0.04	−12.04 ± 0.07	1.33	1.26	silver	
15zi	204.267489	−29.802396	M83	1771	−10.90 ± 0.06	−12.04 ± 0.08	2.49	2.03	silver	
16dr	204.303412	−29.85154	M83	1509	−11.05 ± 0.07	−12.04 ± 0.05	1.52	1.66	silver	2
14ni	148.873272	69.114964	M81	1408	−11.05 ± 0.09	−12.01 ± 0.11	2.44	1.19	bronze	17
15kb	204.186924	−29.863754	M83	1458	−11.34 ± 0.03	−12 ± 0.02	1.17	1.28	gold	
…										

Note. Description of columns. *Name*: SPIRITS name for variable; *R.A.* and *decl.*: R.A. and decl. (in degrees for equinox 2000); *Gal*: galaxy Name; *Period*: period in days; [3.6]: 3.6 μm mean absolute magnitude; [4.5]: 4.5 μm mean absolute magnitude; Δ[3.6]: 3.6 μm amplitude (mag); Δ[4.5]: 4.5 μm amplitude (mag); *Quality*: subjective classification for variable; *References*: associations with clusters or other catalogs.

References. [1]: Grammer & Humphreys (2013), [2]: Page et al. (2014), [3]: Donovan Meyer et al. (2013), [4]: Larsen (2004), [5]: Lee et al. (2011), [6]: Ryon et al. (2015), [7]: Flesch (2017), [8]: Vucetic et al. (2015), [9]: Silva-Villa & Larsen (2011), [10]: Drazinos et al. (2013), [11]: Larsen (2011), [12]: Blair et al. (2012), [13]: Hadfield et al. (2005), [14]: Mora et al. (2009), [15]: Larsen (1999), [16]: Nasa & Heasarc (2018), [17]: Khan et al. (2010).

(This table is available in its entirety in machine-readable form.)

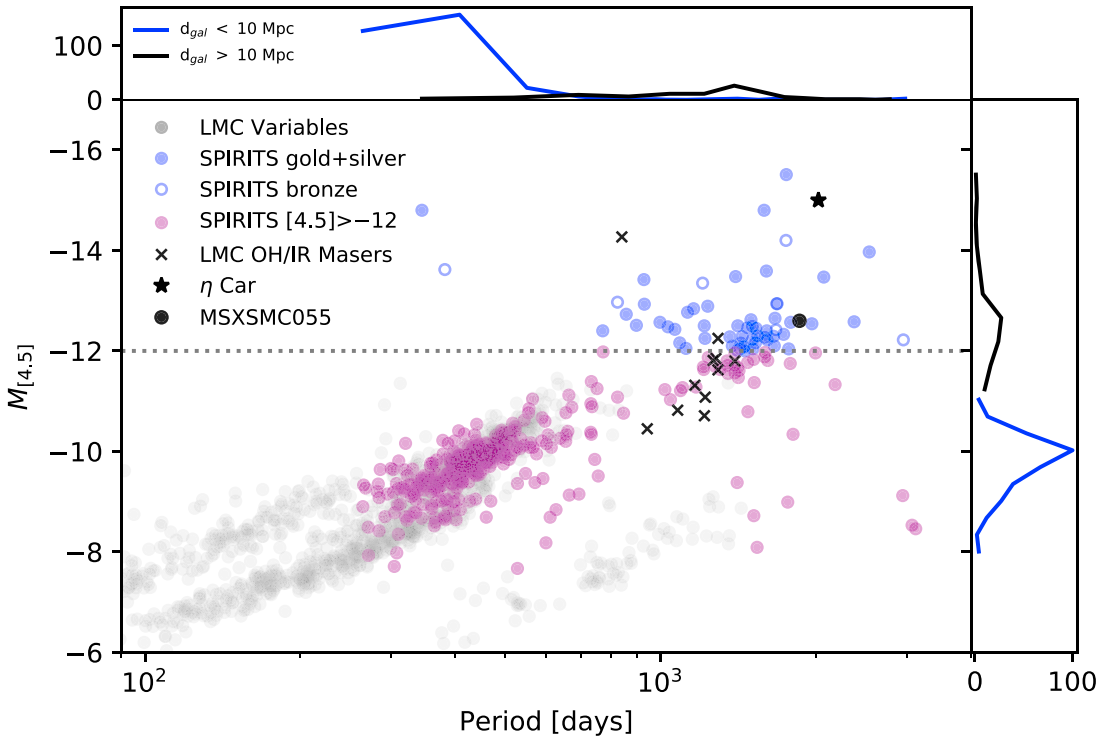

Figure 3. Period–luminosity diagram for the SPIRITS variables. The dotted line distinguishes the brightest variables ($M_{[4.5]} < -12$), which we discuss in Section 3.2. Many of the fainter variables ($M_{[4.5]} > -12$) are probably AGB stars pulsating in the fundamental or first overtone modes. Shown for comparison are the LMC AGB variables (Riebel et al. 2015) and LMC OH/IR sources (Goldman et al. 2017) (the most luminous of these, WOH G64, is a RSG), plus two individual objects discussed in Section 3.3.2. The value of $M_{[4.5]} = -15.0$ used for η Car is the mean of the 4.2 and 4.9 μm measurements from Price & Murdock (1983) and Ney & Merrill (1980), respectively, and assumes a distance of 2300 pc (although possibly it is more distant Davidson et al. 2018). MSX-SMC-055 is both a candidate super-AGB star and a candidate TZO; its magnitude $M_{[4.5]} = -12.6$ is from Boyer et al. (2011). In the top and right panels, we plot the histograms of the periods and luminosities of SPIRITS variables, respectively. The blue histograms represent the variables in nearby ($d < 10$ Mpc) galaxies, and the black histograms represent variables in distant ($d > 10$ Mpc) galaxies. As is evident, we have a bimodal distribution of variables, where the shorter-period to lower-luminosity variables preferentially belong to the nearby galaxies, and the longer-period, more luminous variables belong to the distant, more massive galaxies. This apparent bimodal distribution is a consequence of our limited sensitivity, in that we are not sensitive to the low-luminosity variables from the distant massive galaxies, and the nearby galaxies have much lower stellar masses, and are thus unlikely to host the long-period luminous variables.

gap may be an artifact of the differing sensitivities of our two-tiered galaxy sample. While our cadence and light-curve durations maintain sensitivity to periods between 650 and 1200 days, the survey is not sensitive to variables fainter than $M_{[4.5]} \sim -11$ (see Figure 1) in the massive, more distant galaxy sample. Since the stellar mass in the massive galaxy sample is $\sim$1000$\times$ that of the nearby dwarf sample, the luminous ($M_{[4.5]} < -12$) variables are clearly much rarer than the fainter variables identified in the nearby sample. If variables in the apparent period–luminosity gap are similarly as rare as the luminous variables, the observed gap would arise because the nearby dwarfs may only harbor a few of them and they are too faint to be detected in the massive, more distant galaxy sample.

3.3. Brightest Sources

In this section we discuss the 58 sources in our sample with mean absolute 4.5 μm magnitudes brighter than -12. We classify 24 of these sources as "gold," 26 as "silver," and 8 as "bronze" variables (Table 3).

Eleven of these sources have mean $M_{[4.5]}$ luminosities brighter than -13. Of these, 9 have long periods (>900 days): SPIRITS 15js, SPIRITS 15jt, SPIRITS 16do, and SPIRITS 16po in M83, SPIRITS 14apu, SPIRITS 14apz, and SPIRITS 15pk in M101, and SPIRITS 15ty in NGC 6946 and SPIRITS 18ec in M51. Short periods were found for two sources: 344 days for SPIRITS 14aue (Figure 15) in IC 342 and 381 days for SPIRITS 14axv (SN2005at) in NGC 6744. SPIRITS 14apu (Figure 16), the most luminous source in the sample, has a mean absolute $M_{[4.5]} = -15.51$, a period of 1752 days, a [4.5] amplitude of 0.25 mag, and a [3.6]–[4.5] color of 0.58. It is one of the M101 cluster sources discussed below. Two of these extraluminous sources have periods longer than 2000 days: SPIRITS 16do (2071 days, Figure 17) and SPIRITS 18ec (2538 days, Figure 18). Seven of these luminous long-period (>900 days) variables have matches in the 5.8 and 8.0 μm catalogs. These bright sources have reference 8.0 μm magnitudes brighter than -16. They are extremely red with [3.6]–[4.5] colors between 0.42 and 1.48 and reference [3.6]–[8.0] colors between 3.0 and 4.75.

We find 47 sources with mean absolute 4.5 μm magnitudes between -12 and -13. As a representative of this sample, we present the folded light curve of the source SPIRITS 14apq (Figure 19), which has a period of 1606 days and a mean 4.5 μm absolute magnitude of -12.40. The periods of these sources range from 770 to 2956 days. Most of them are extremely red, with [3.6]–[4.5] colors between 0.4 and 1.5. Eighteen of these sources have counterparts in 5.8 and 8.0 μm images. Their reference [8.0] magnitudes range from -13.5 to -17 and their reference [3.6]–[8.0] colors lie between 1.5 to 4.5.

There is a group of variables that overlap the longest period LMC OH/IR stars in Figure 3. These have periods between 1300 and 1800 days and absolute 4.5 μm magnitudes between -11.5 and -12.5. We represent them by the phase-folded light

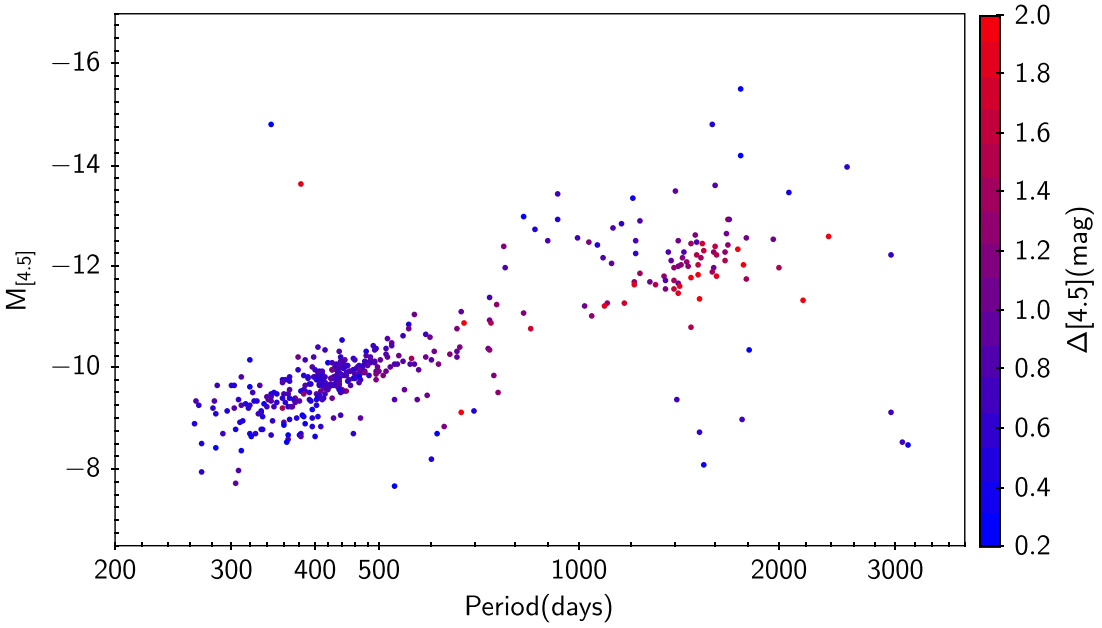

Figure 4. Period–luminosity diagram of SPIRITS sources, color-coded by their amplitudes. A majority of our low-luminosity AGB candidates have relatively small amplitudes, from 0.5 to 1 mag. The higher-amplitude sources are found predominantly at higher luminosities and longer periods. The group around $P \sim 1500$ days and $M_{[4.5]} \sim -12$, which we think are relatively massive AGB stars, have particularly large amplitudes.

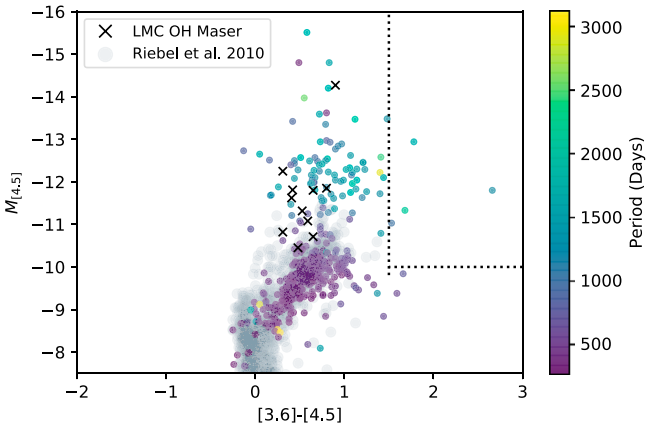

Figure 5. Mean $M_{[4.5]}$ vs. [3.6]–[4.5] color–magnitude diagram for SPIRITS variables, along with LMC AGB variables (smaller red points). The shorter-period and lower-luminosity variables in our sample coincide with the LMC variables, and hence are most likely AGB stars. The more luminous and longer-period variables are clearly separated from the AGB region in the diagram. These sources have colors ranging from −0.5 to 1.5. Some of them occupy the same part of the color–magnitude diagram as LMC OH Masers (black crosses). We also indicate the SN2008s-like region of Thompson et al. (2009) (M [4.5] < -10 and [3.6]–[4.5] > 1.5 mag). There are three variable sources in this extremely red region.

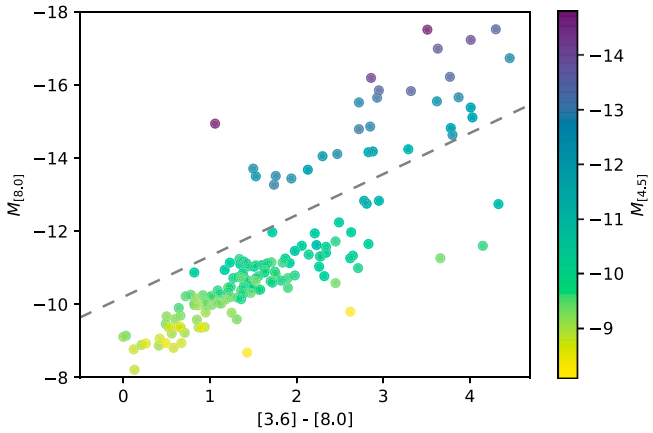

Figure 6. Reference [8.0] vs. [3.6]–[8.0] CMD for the SPIRITS variables, color-coded by their $M_{[4.5]}$. We note that our AGB candidates exhibit a sequence, while the luminous ([4.5] brighter than −12) candidates lie on a different, more luminous sequence. The gray line roughly indicates the separation of these two sequences. However, most of the luminous sources belong to clusters or are near H II regions. This, coupled with the fact that the PSF is large at 8.0 μm, could inflate the brightness and colors of these sources.

curve of the source SPIRITS 15kb (Figure 20) in the galaxy M83. SPIRITS 15kb has a period of 1458 days and a mean absolute 4.5 μm magnitude of −12. This group of sources has large amplitudes, larger in general than than the even brighter ($M_{[4.5]} < -13$) sources. These are probably AGB stars with massive progenitors.

Kwon & Suh (2010) present an empirical M- and L-band amplitude–period relation using 12 galactic OH/IR stars. We compare the $M_{[4.5]}$ and the $M_{[3.6]}$ amplitude–period relation for SPIRITS variables to the M- and L-band relations, respectively, in Figure 21. While our lower-luminosity variables are found in the low-period/low-amplitude region, the longer-period variables show a huge spread in amplitude. We note that *MSX* SMC055, the super-AGB and TZO candidate discussed in Section 3.3.2, has a modest amplitude ($\Delta L \sim 0.7$ mag) compared to the Galactic OH/IR stars. At least some of the high-luminosity variables are candidates for OH/IR Masers.

Some of the brightest SPIRITS sources have been identified in other catalogs and have Two Micron All Sky Survey (Milligan et al. 1996), *Wide-field Infrared Survey Explorer* (Wright et al. 2010), and Panoramic Survey Telescope and Rapid Response System (Kaiser et al. 2002) photometry. The last column of Table 3 contains references for specific sources, where they are associated with clusters, H II regions, SN remnants, etc.

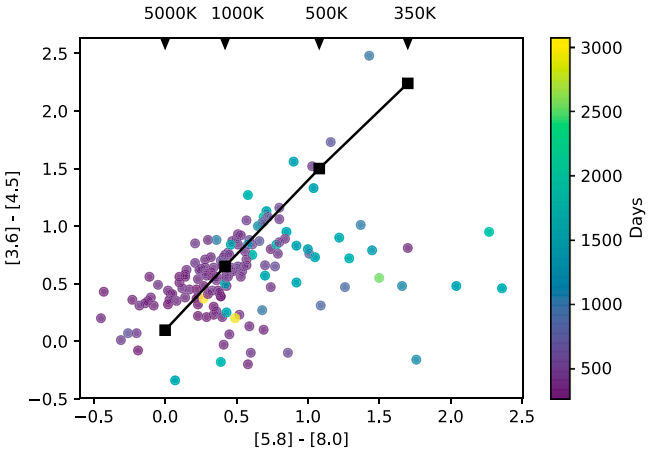

Figure 7. Color–color diagram for SPIRITS sources. The black line and squares denote the expectation for a blackbody of temperature 5000, 1000, 500, and 350 K. The sources that lie below the blackbody line have an IR excess due to the dust enshrouding them. A colder dust shell pushes a star to the bottom right of this diagram, with larger [5.8]–[8.0] colors.

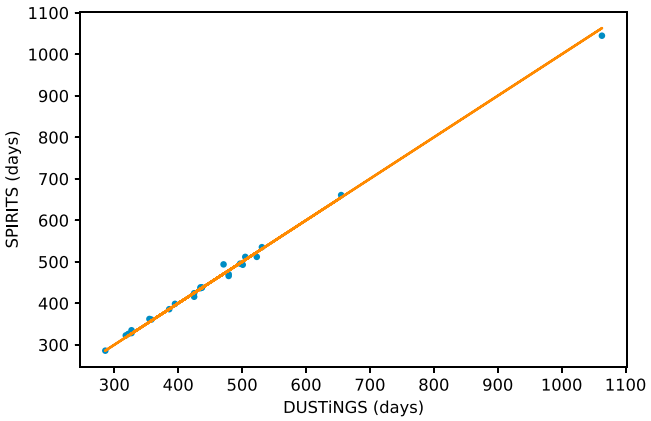

Figure 8. Comparison of SPIRITS and DUSTiNGS periods.

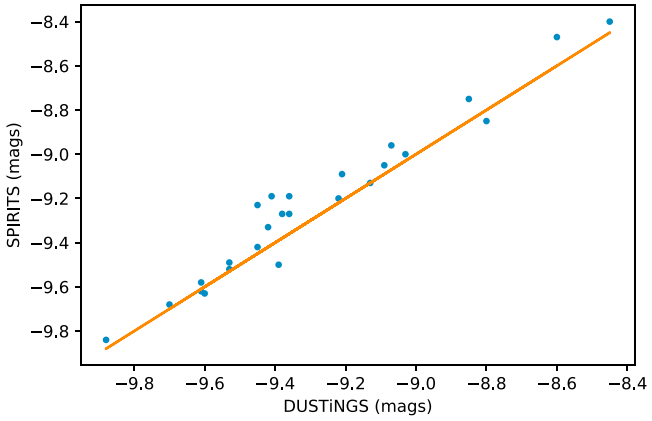

Figure 9. Comparison of SPIRITS and DUSTiNGS 3.6 μm absolute magnitudes.

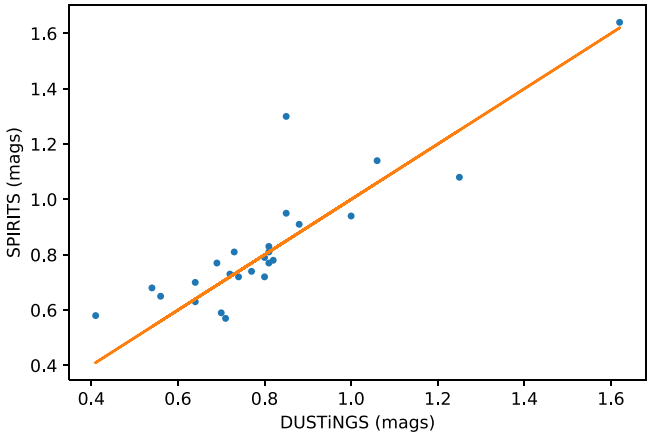

Figure 10. Comparison of SPIRITS and DUSTiNGS 3.6 μm amplitudes.

3.3.1. Variables in Clusters

A large fraction of the most luminous variables ($M_{[4.5]}$ brighter than −12) in M101 and M83 may be associated (some in, others nearby) with star clusters. Some of the luminous variables not obviously associated with clusters are very close to H II regions (e.g., 18ec in M51, Lee et al. 2011), giant molecular clouds (e.g., 15ty in NGC 6946, Donovan Meyer et al. 2013) and/or SNe remnants (e.g., 15jt in M83, Winkler et al. 2017), and it is not possible to determine if they are associated with clusters as well. Most of the other galaxies with luminous variables have not been surveyed with *HST*, so no comparison can be made. The brightest sources, those with $M_{[4.5]}$ brighter than −13, are probably RSGs. So we expect that most of them will be found in clusters, and that these clusters would be unresolved by *Spitzer*. Accordingly, the magnitudes of these sources are likely somewhat inflated by the light of the rest of the cluster. However, 4 of these 11 brightest variables vary by more than 50%, meaning their phase-weighted mean magnitudes are dominated by the variable and not the cluster light.

Grammer & Humphreys (2013) discussed the massive star population in M101 from *HST* photometry. Of our 12 very luminous variables in M101, 10 are coincident with large numbers of their massive stars, with between 13 and 155 stars within a radius of three arcseconds of the *Spitzer* position. There are only a few red supergiants ($V < 24$, $V - I > 1.2$) among these, but we would not expect very dusty sources to show up at *HST* wavelengths. There is no optical counterpart in the *HST* images at the positions of the other two sources (SPIRITS 14bco and SPIRITS 18ae) in M101. Grammer et al. (2015) examined some of the massive stars in more detail, obtaining spectra and looking for variability. They found various hot and warm supergiants, LBVs, and Wolf-Rayet (WR) candidates. None of their variables are close to the sources we discuss.

Silva-Villa & Larsen (2011) discussed clusters in M83 and three other galaxies using *HST* photometry. As indicated in Table 3, five variables may be associated with one or more suspected or accepted cluster in M83, although not as closely associated as the M101 sources are with their clusters. Silva-Villa & Larsen (2011) suggested these M83 clusters are of intermediate age, $10^8 < \text{age} < 10^9$ yr and intermediate total mass, $10^{3.3} < M < 10^{4.4}\ M_\odot$, noting that it is difficult to estimate age or mass for these clusters. Ryon et al. (2015) also discussed clusters in M83, three of which are among our sample, two in common with Silva-Villa & Larsen (2011). They found slightly younger ages, $<10^{8.5}$ yr, and comparable masses for the three of interest. Larsen (2011) presented color–magnitude diagrams of a few individual clusters, including NGC5236-F1-3 in M83, which coincides with SPIRITS 15zg. They derived an age of $10^{7.5}$ yr for this cluster. We note that at the distance of M83 a star traveling at the modest velocity of 30 km s^{-1} would take only about

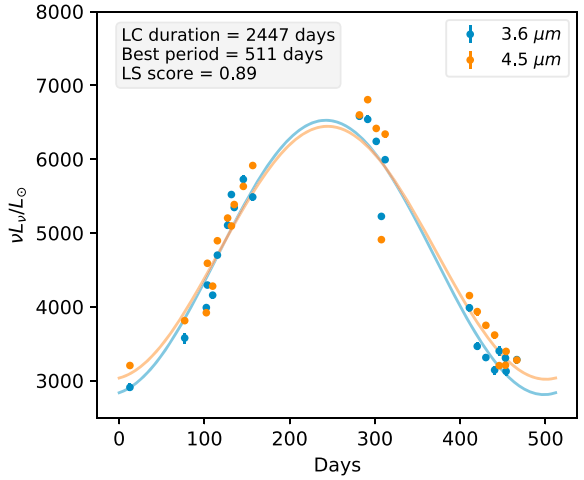

Figure 11. Phase−folded light curve of SPIRITS 14va: WLM. This source has a $M_{[4.5]} = -10.26$, $\Delta[3.6] = 0.91$, $\Delta[4.5] = 0.82$ and is a representative of the AGB candidates in our sample that appears in the same region as the LMC fundamental mode AGB variables in Figure 3.

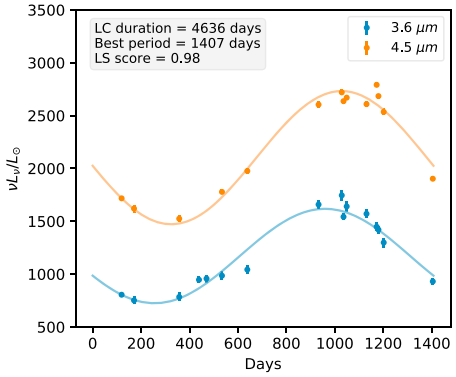

Figure 12. Phase−folded light curve of SPIRITS 15acg,: NGC 185, one of the long- period AGB candidates, that extends the long-period sequence of LMC variables in Figure 3 to higher periods. This source has $M_{[4.5]} = -9.38$, $\Delta[3.6] = 0.87$ and $\Delta[4.5] = 0.67$.

2×10^6 yr to travel three arcseconds and could therefore have moved a long way from the birth site in 10^7–10^8 yr. A more detailed study is required to establish if these stars were flung out of clusters some distance from where they now are.

If the ages mentioned above for M83 are correct we would not expect to see red supergiants or very luminous AGB stars, which will not be older than about 10^8 yr. The clusters in M101 could certainly include RSGs and/or super-AGB stars. Interacting binaries are of course possible, and even likely, in both galaxies.

3.3.2. Binaries

It seems almost certain that some of these luminous variables will be interacting binaries. A comprehensive discussion of the numerous alternatives is beyond the scope of this discovery paper, but we do briefly examine a few possibilities. We start with η Car, which is a very massive star (around 100 $M_\odot$) in a highly eccentric binary system (Damineli 1996), which varies on many timescales and emits at every wavelength (see, e.g., Davidson & Humphreys 2012, and references therein). It is often classified as an LBV, although it differs significantly

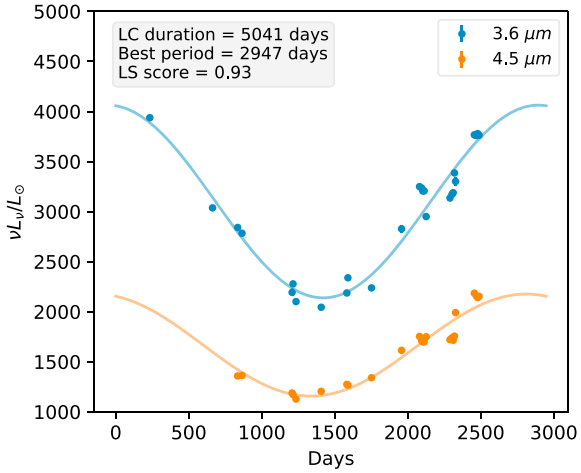

Figure 13. Phase−folded light curve of SPIRITS 14ct: NGC 6822, one of the long- period AGB candidates; see also Figure 25. This source has $M_{[4.5]} = -9.12$, $\Delta[3.6] = 0.7$, and $\Delta[4.5] = 0.69$

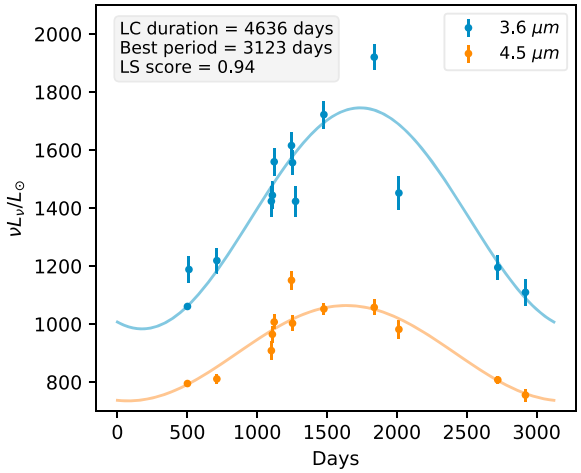

Figure 14. Phase−folded light curve of SPIRITS 15aci: NGC 185, the AGB candidate with the longest period, that extends the long-period sequence of LMC variables in Figure 3 to longer periods. This source has $M_{[4.5]} = -8.46$, $\Delta[3.6] = 0.62$, and $\Delta[4.5] = 0.4$.

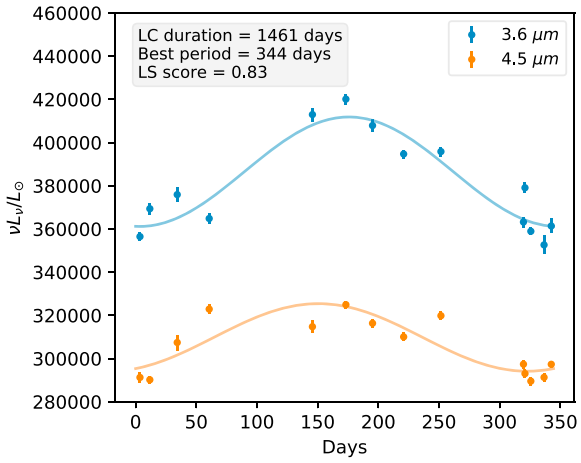

Figure 15. Phase−folded light curve of SPIRITS 14aue: IC342. This source is one of the two high-luminosity ($M_{[4.5]}$ brighter than −13), low-period variables in our sample, placed at the center of Figure 3. This source has $M_{[4.5]} = -14.8$, $\Delta[3.6] = 0.91$, and $\Delta[4.5] = 0.11$.

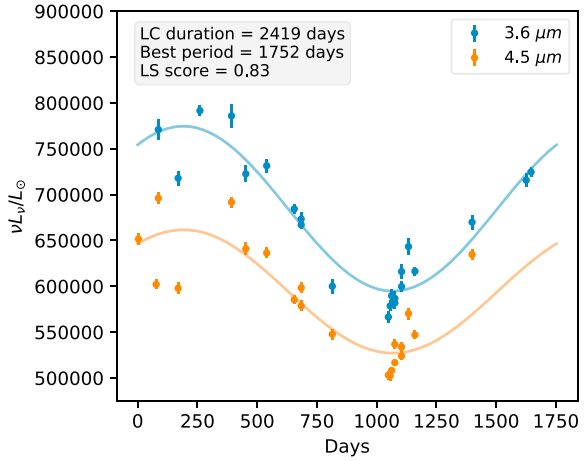

Figure 16. Phase−folded light curve of SPIRITS 14apu: M101, the brightest source in our sample, with $M_{[4.5]} = -15.51$, $\Delta[3.6] = 0.29$, and $\Delta[4.5] = 0.25$.

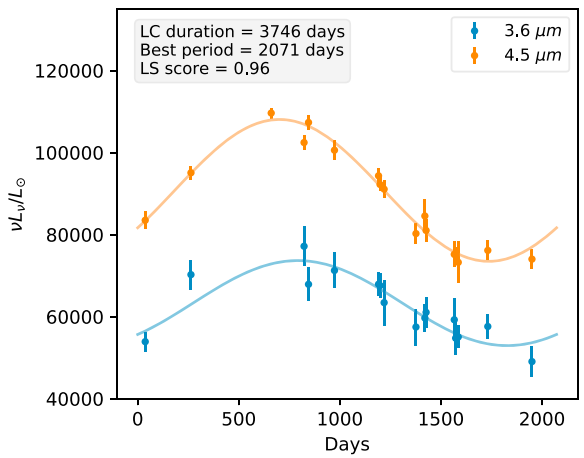

Figure 17. Phase−folded light curve of SPIRITS 16do: NGC 5236, one of the most luminous sources ($M_{[4.5]}$ brighter than −13) in our sample, with an extremely long period (>2000 days). This source has $M_{[4.5]} = -13.47$, $\Delta[3.6] = 0.36$, and $\Delta[4.5] = 0.42$.

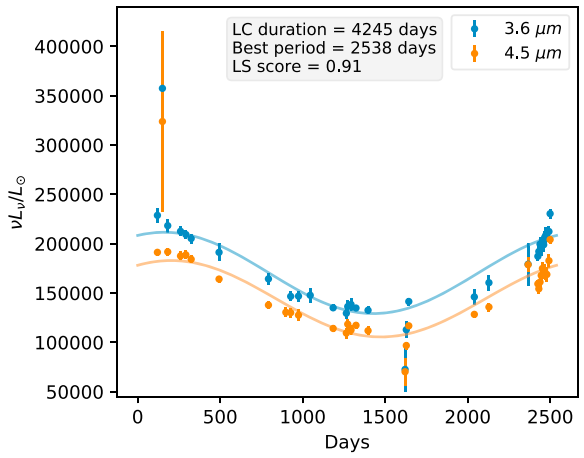

Figure 18. Phase−folded light curve of SPIRITS 18ec: NGC 5194, one of the most luminous sources ($M_{[4.5]}$ brighter than −13) in our sample, with an extremely long period (>2500 days). This source has $M_{[4.5]} = -13.97$, $\Delta[3.6] = 0.54$, and $\Delta[4.5] = 0.6$.

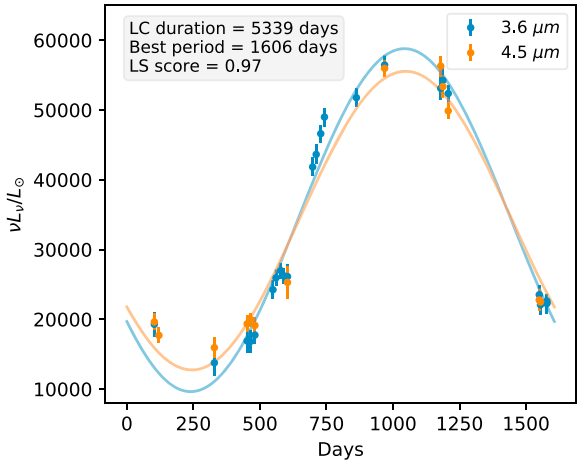

Figure 19. Phase−folded light curve of SPIRITS 14apq: M81, representative of sources with $M_{[4.5]}$ between −12 and −13. This source has −12.4, $\Delta[3.6] = 1.96$, and $\Delta[4.5] = 1.6$.

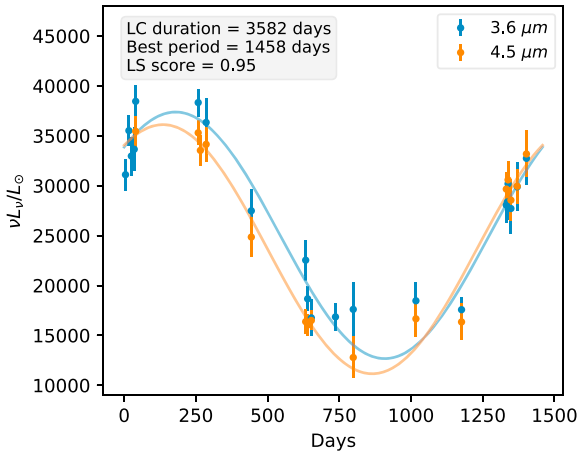

Figure 20. Phase−folded light curve of SPIRITS 15kb: NGC 5236. This source belongs to the group of variables around the LMC Masers in Figure 3 and has $M_{[4.5]} = -12$, $\Delta[3.6] = 1.17$ and $\Delta[4.5] = 1.28$.

from other LBVs (e.g., most of the others are blue and very few are known binaries). Even if such massive stars are very rare, η Car is extremely red (its mass-loss rate exceeds $10^{-3}\ M_\odot\ \mathrm{yr}^{-1}$ (e.g., Hillier et al. 2001)) and extremely luminous and similar objects should be anticipated in a mid-infrared survey of galaxies with large populations of very young stars; although confusion within star-forming regions will probably present challenges. η Car has an L amplitude of about 0.4 (Whitelock et al. 2004) and is shown in Figure 3 at the orbital period of 2023 days. However, we note that the character of the variations is somewhat different from those of most of the SPIRITS variables, in that the η Car variation is concentrated around the time of periastron. Other LBVs are much less luminous in the infrared, although some have exhibited quasi-periodicity on the timescale under discussion.

A majority of late-type Carbon-rich Wolf-Rayet (WCL) binaries are efficient dust producers ($\dot{M} \gtrsim 10^{-8}\ M_\odot\ \mathrm{yr}^{-1}$, Williams et al. 1987) and large-amplitude IR variables (e.g., Williams et al. 1990). Dust production in these systems is thought to originate from the compression of stellar winds in shocked wind-collision regions between the WC star and a

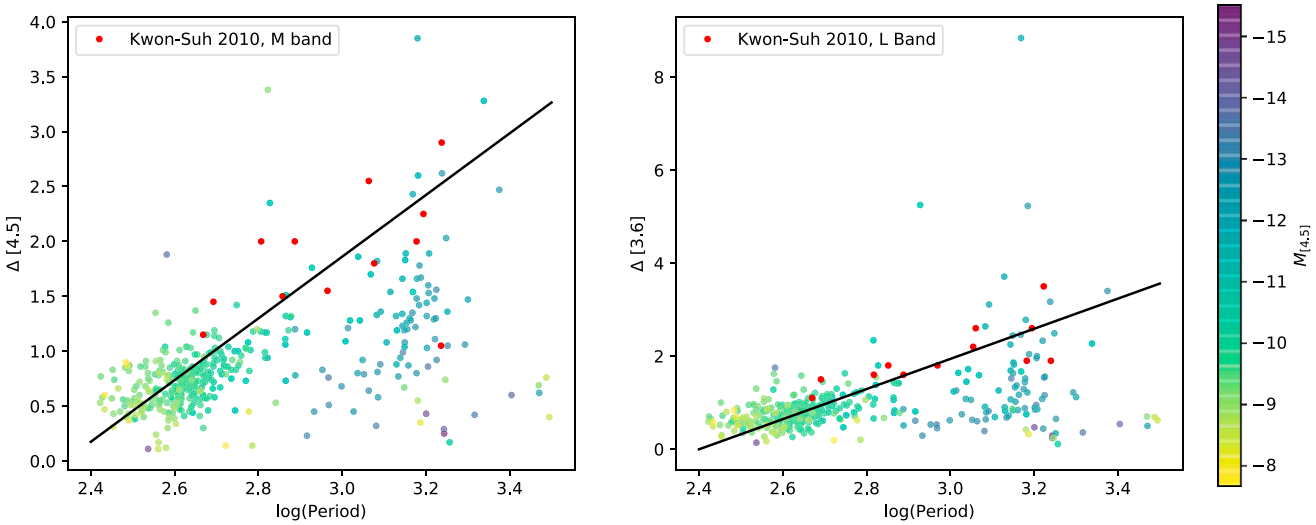

Figure 21. Here, we compare our variables with the *L*- and *M*-band amplitude–period relation (black solid line) derived by Kwon & Suh (2010) for Galactic OH/IR Masers (red dots). While our lower-luminosity variables are found in the low period–low-amplitude region, the higher luminosity variables show a large spread. Some of these could have circumstellar maser emission.

luminous O or B companion (Usov 1991). Some dusty WC systems therefore exhibit periodic or episodic IR brightening events corresponding to dust production. For example, the archetypal periodic dust-making Wolf-Rayet binary WR140 (WC7+O5I), located at $d = 1.67 \pm 0.03$ kpc (Monnier et al. 2011), has an eccentric orbit and exhibits IR outbursts during periastron passage in its 7.94 yr orbit (Williams et al. 2009). WR140 has mean infrared magnitudes of $L = 3.5$ and $M = 3.3$ and an amplitude $\Delta M = 2.4$ (Williams et al. 2009; Taranova & Shenavrin 2011). On Figure 3 this would put it among the very longest period variables with $M_{[4.5]} \sim -8$, but there are more IR luminous WR binaries. The variable, dusty "pinwheel" system WR 98a (WC8-9) (Monnier et al. 1999) is located at $d = 1.9$ kpc and exhibits a mean infrared magnitude of $L = 1.5$ ($M_{[3.6]} \sim -10$) with a 1.6 yr orbital period (Williams et al. 1995). One of the most IR luminous WR binaries, WR 48a (WC8 + O), shows periodic variability on 32 yr timescales with peak L' and M magnitudes of 0.1 and -0.7, respectively (Williams et al. 2012). At a distance of 4 kpc, the absolute IR magnitude of WR48a is $M_{[4.5]} \sim -14$, which is consistent with some of the brightest variables in Figure 3.

Some WR binary systems exhibit a different type of variability: deep optical eclipses that do not phase with their orbital period (Williams 2014). Unlike the periodic variability linked to enhanced dust formation at periastron, the erratic eclipses are likely due to obscuration by dust formed in clumps along the line of sight. WR104, a WC9+O binary surrounded by the Pinwheel Nebula (Tuthill et al. 1999), has $[3.6] = -0.13$ and $[4.8] = -1.01$ (Gehrz & Hackwell 1974; Williams et al. 1987) and exhibits large amplitude and erratic optical variability (Williams 2014). However, there is only limited information on its infrared variability. Using a distance of 2.58 ± 0.12 kpc (Soulain et al. 2018), we estimate $M_{[4.5]} \sim -13$, i.e., comparable to the brightest variables under discussion (the *Gaia* DR2 parallax, which has a large uncertainty, would make it more distant and hence even brighter).

It is not easy to identify stars in the common-envelope phase that must be the penultimate stage in the evolution of many types of close binary (Han et al. 1995). One-dimensional hydrodynamic simulations (Clayton et al. 2017) of low-mass red giants undergoing a common-envelope event indicate that their envelopes become unstable and develop large-amplitude pulsations; these may be quasi-periodic and can drive high mass-loss rates. Glanz & Perets (2018) also discussed the similarity of common-envelope stars to pulsating AGB stars, and how dust could form in their extended atmospheres and drive high mass-loss rates. The TZOs are postulated examples of common-envelope evolution. These would be neutron stars embedded in an extended hydrogen envelope that form from a massive binary after one star explodes as a supernova and its remnant core becomes embedded in a common envelope with its companion (Thorne & Zytkow 1975). It has also been suggested that LBVs could be TZOs (King 2000).

Figure 3 shows the SMC source *MSX* SMC055 (IRAS 00483 −7347), which is both a super-AGB candidate (Groenewegen et al. 2009) and a TZO candidate (Levesque et al. 2014). Deriving the initial mass of the star from the available data is not trivial and it is therefore not possible to be certain which of these interpretations is correct. *MSX* SMC055 has a period of 1859 days (Soszyński et al. 2011) and an *L* amplitude of 0.7 (Menzies et al. 2019) and in Figure 2 it falls very close to the clump of SPIRITS variables that seem to be on an extension of the AGB fundamental sequence. We therefore suggest that these may be super-AGB stars (and/or TZOs).

4. Summary

We present a catalog of 417 luminous IR variable candidates in 20 nearby luminous galaxies targeted by the ongoing SPIRITS survey. We report the periods, mean magnitudes, and the reference photometry for these variables. We also present the IRAC 3.6, 4.5, 5.8, and 8.0 μm PSF catalogs for reference images of all 20 host galaxies. Over 300 of these are AGB candidates, based on their positions in the period–luminosity and color–magnitude diagrams.

In addition to these, we find about 50 variables that are more luminous and have longer periods than those from previous surveys. The majority of these have $1000 < P < 2000$ and $M_{[4.5]}$ between -11 and -13, and fall near the extrapolation of the relation for fundamental pulsation in the period–luminosity

diagram. This suggests that these are AGB stars with massive progenitors, certainly more massive than those of the LMC OH/IR stars, and perhaps even super-AGBs. The sample with $M_{[4.5]}$ brighter than -12 will include some RSGs with high mass-loss rates and probably exotic examples of interacting binaries, e.g., TZOs. There are also nine LPVs with $M_{[4.5]}$ brighter than -13, that lie in a previously unexplored region of the period–luminosity diagram; several of these are located within young clusters. The extraluminous variables will include some contamination that is inevitable given our limited spatial resolution, but some of these sources could also be part of a new, previously unknown class of variables. Exploring the true nature of these extraluminous variables will be an exciting avenue of exploration for future missions, such as the *James Webb Space Telescope*.

We thank Dave Cook, Maria Drout, Shazrene Mohamed, and John Menzies for useful discussions. This work is based on observations made with *Spitzer*, which is operated by the Jet Propulsion Laboratory, California Institute of Technology under a contract with NASA. The SPIRITS team acknowledges generous support from the NASA *Spitzer* grants for SPIRITS. P.A.W. thanks the South African NRF for research funding. J.E.J. acknowledges support from the National Science Foundation Graduate Research Fellowship under grant No. DGE-1144469. R.D.G. was supported by NASA and the United States Air Force. This research has made use of the VizieR catalog access tool, CDS, Strasbourg, France. The original description of the VizieR service was published in A&AS 143, 23. This work has made use of data from the European Space Agency (ESA) mission *Gaia* (https://www.cosmos.esa.int/gaia), processed by the *Gaia* Data Processing and Analysis Consortium (DPAC, https://www.cosmos.esa.int/web/gaia/dpac/consortium). Funding for the DPAC has been provided by national institutions, in particular the institutions participating in the *Gaia* Multilateral Agreement.

Appendix

As described in Section 2.4, we assign a quality (gold, silver or bronze) to each of our bright variables based on visual inspection of light curves and periodograms. Here, we discuss some of the interesting variables in the bronze classification.

The source SPIRITS 15pk (Figure 22) is not a periodic variable with a period of 1750 days, but probably a brief flare (of ≈27 days). It is situated within a massive star cluster in M101 (Grammer & Humphreys 2013). While low-mass YSOs are not prone to luminous outbursts, massive protostars can exhibit such flares and could be responsible for the brief outburst observed in this source. Bally et al. (2017) posit that a merger of a highly enshrouded protostar and a 15 $M_{\odot}$ radio source could have powered a high-energy (10^{48} erg) explosion in the Orion OMC1 region about 500 yr ago, producing a luminous infrared transient. Massive star mergers in star-forming regions could also result in high-energy outbursts (Bally & Zinnecker 2005). Periodic flares are also possible in systems in which a massive companion has an eccentric, non-coplanar orbit with respect to a disk around the primary.

The light curves of SPIRITS 14axv (SN2005at Figure 23) and SPIRITS 14bkv (Figure 24) are characterized by the presence of one epoch separated in time distinctly from the remaining light curve, which drives the period finding

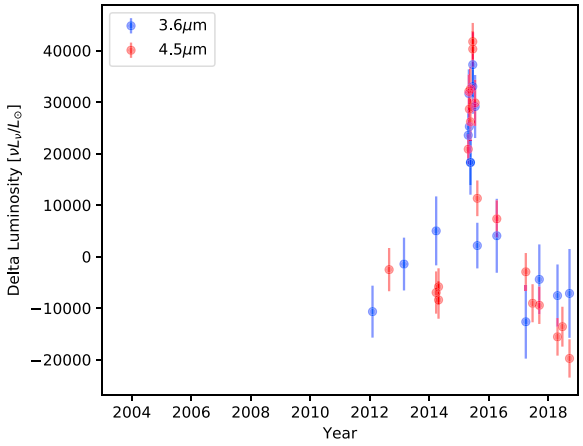

Figure 22. SPIRITS 15pk: M101. This source is not a periodic variable, but seems to flare briefly.

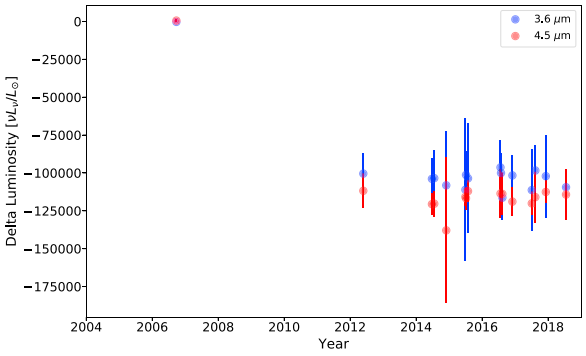

Figure 23. SPIRITS 14axv: NGC 6744. This source has one epoch from the reference image separated from the rest of the light curve, which drives the period finding algorithm. The source is SN2005at; it is obviously not periodic and only detected at the first epoch.

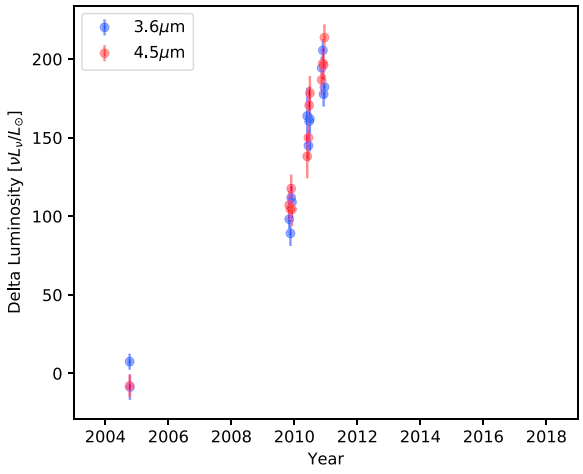

Figure 24. SPIRITS 14bkv: NGC 6822. This source has one epoch separated from the majority of the light curve, and this point influences the period we find. Many more observations are required to determine if this source is actually periodic.

algorithm. More data are required to identify the period of SPIRITS 14bkv, while SPIRITS 14axv is not a periodic source, but coincident (within 1.″1) with SN2005at (Lennarz et al. 2012). Lastly, our data permit reliable determination of periods longer than 250 days only. Hence, it is possible that the

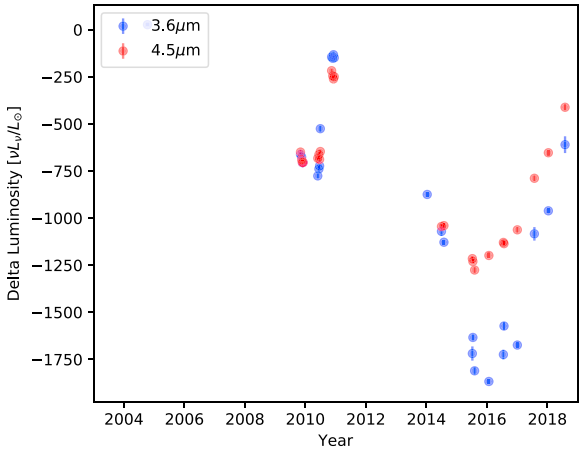

Figure 25. SPIRITS 14ct: NGC 6822. The light curve suggests shorter periods in addition to the 2947 days found in our analysis; see also Figure 13.

primary period in some of our variables is shorter than 250 days and that the value we report is erroneous. The light curve of SPIRITS 14ct (Figures 25 and 13) either has a shorter period or erratic variations superimposed on the 2947 days we determine. It also has large-amplitude *JHK* variations and has been classified as a C-star (Whitelock et al. 2013). The source SPIRITS 14aud, for which we determine a period of 694 days, is coincident with the Cepheid V22 having a period of 146 days (Sandage 1971). SPIRITS 14bge is variable and we report a period of 402 days; however, the data (not illustrated) are insufficient for any period to be determined. These examples indicate the limitations of our classification criteria. They are all plotted in Figure 3 at the periods we determined and therefore make a minor contribution to the scatter.

ORCID iDs

P. A. Whitelock https://orcid.org/0000-0002-4678-4432
M. M. Kasliwal https://orcid.org/0000-0002-5619-4938
J. E. Jencson https://orcid.org/0000-0001-5754-4007
M. L. Boyer https://orcid.org/0000-0003-4850-9589
S. R. Goldman https://orcid.org/0000-0002-8937-3844
F. Masci https://orcid.org/0000-0002-8532-9395
A. M. Cody https://orcid.org/0000-0002-3656-6706
J. Bally https://orcid.org/0000-0001-8135-6612
H. E. Bond https://orcid.org/0000-0003-1377-7145
R. D. Gehrz https://orcid.org/0000-0003-1319-4089

References

Alcock, C., Allsman, R. A., Axelrod, T. S., et al. 1993, in ASP Conf. Ser. 43, Sky Surveys. Protostars to Protogalaxies, ed. B. T. Soifer (San Francisco, CA: ASP), 291
Bally, J., Ginsburg, A., Arce, H., et al. 2017, ApJ, 837, 60
Bally, J., & Zinnecker, H. 2005, AJ, 129, 2281
Blair, W. P., Winkler, P. F., & Long, K. S. 2012, ApJS, 203, 8
Boyer, M. L., Srinivasan, S., van Loon, J Th., et al. 2011, AJ, 142, 103
Boyer, M. L., McQuinn, K. B. W., Barmby, P., et al. 2015, ApJ, 800, 51
Clayton, M., Podsiadlowski, P., Ivanova, N., & Justham, S. 2017, MNRAS, 470, 1788
Damineli, A. 1996, ApJL, 460, L49
Davidson, K., Helmel, G., & Humphreys, R. M. 2018, RNAAS, 2, 133
Davidson, K., & Humphreys, R. M. (ed.) 2012, Eta Carinae and the Supernova Impostors, Vol. 384 (Boston, MA: Springer)
De Marco, O., & Izzard, R. G. 2017, PASA, 34, e001
Doherty, C. L., Gil-Pons, P., Siess, L., & Lattanzio, J. C. 2017, PASA, 34, e056
Doherty, C. L., Gil-Pons, P., Siess, L., Lattanzio, J. C., & Lau, H. H. B. 2015, MNRAS, 446, 2599
Donovan Meyer, J., Koda, J., Momose, R., et al. 2013, ApJ, 772, 107
Drazinos, P., Kontizas, E., Karampelas, A., Kontizas, M., & Dapergolas, A. 2013, A&A, 553, A87
Fazio, G. G., Hora, J. L., Allen, L. E., et al. 2004, ApJS, 154, 10
Feast, M. W., Glass, I. S., Whitelock, P. A., & Catchpole, R. M. 1989, MNRAS, 241, 375
Flesch, E. W. 2017, yCat, 7280, 0
Gaia Collaboration et al. 2019, A&A, 623, A110
Gehrz, R. D., & Hackwell, J. A. 1974, ApJ, 194, 619
Gehrz, R. D., Roellig, T. L., Werner, M. W., et al. 2007, RScI, 78, 011302
Glanz, H., & Perets, H. B. 2018, MNRAS, 478, L12
Goldman, S. R., van Loon, J. Th., Zijlstra, A. A., et al. 2017, MNRAS, 465, 403
Goldman, S. R., van Loon, J. Th., Gómez, J. F., et al., et al. 2018, MNRAS, 473, 3835
Grammer, S., & Humphreys, R. M. 2013, AJ, 146, 114
Grammer, S. H., Humphreys, R. M., & Gerke, J. 2015, AJ, 149, 152
Groenewegen, M. A. T., Sloan, G. C., Soszyński, I., & Petersen, E. A. 2009, A&A, 506, 1277
Hadfield, L. J., Crowther, P. A., Schild, H., & Schmutz, W. 2005, A&A, 439, 265
Han, Z., Podsiadlowski, P., & Eggleton, P. P. 1995, MNRAS, 272, 800
Hillier, D. J., Davidson, K., Ishibashi, K., & Gull, T. 2001, ApJ, 553, 837
Hughes, S. M. G., & Wood, P. R. 1990, AJ, 99, 784
Ita, Y., Matsunaga, N., Tanabé, T., et al. 2018, MNRAS, 481, 4206
Kaiser, N., Aussel, H., Burke, B. E., et al. 2002, Proc. SPIE, 4836, 154
Karachentsev, I. D., Makarov, D. I., & Kaisina, E. I. 2013, AJ, 145, 101
Kasliwal, M. M., Bally, J., Masci, F., et al., et al. 2017, ApJ, 839, 88
Khan, R. 2017, ApJS, 228, 5
Khan, R., Stanek, K. Z., Kochanek, C. S., & Sonneborn, G. 2015, ApJS, 219, 42
Khan, R., Stanek, K. Z., Prieto, J. L., et al. 2010, ApJ, 715, 1094
King, N. L. 2000, PhD thesis, New Mexico State Univ.
Kwon, Y.-J., & Suh, K.-W. 2010, JASS, 27, 279
Larsen, S. S. 1999, A&AS, 139, 393
Larsen, S. S. 2004, A&A, 416, 537
Larsen, S. S. 2011, in Stellar Clusters & Associations: A RIA Workshop on Gaia, ed. E. J. Alfaro Navarro, A. T. Gallego Calvente, & M. R. Zapatero Osorio (Palo Alto, CA: Issuu Inc.), 75
Lee, J. C., Gil de Paz, A., Kennicutt, R. C. Jr, et al. 2011, ApJS, 192, 6
Lennarz, D., Altmann, D., & Wiebusch, C. 2012, A&A, 538, A120
Letarte, B., Demers, S., Battinelli, P., & Kunkel, W. E. 2002, AJ, 123, 832
Levesque, E. M., Massey, P., Żytkow, A. N., & Morrell, N. 2014, MNRAS, 443, L94
Lomb, N. R. 1976, Ap&SS, 39, 447
Matsuura, M., Barlow, M. J., Zijlstra, A. A., et al. 2009, MNRAS, 396, 918
McQuinn, K. B. W., Woodward, C. E., Willner, S. P., et al., et al. 2007, ApJ, 664, 850
Meixner, M., Gordon, K. D., Indebetouw, R., et al. 2006, AJ, 132, 2268
Menzies, J. W., Whitelock, P. A., & Feast, M. W. 2015, MNRAS, 452, 910
Menzies, J. W., Whitelock, P. A., Feast, M. W., & Matsunaga, N. 2019, MNRAS, 483, 5150
Milligan, S., Cranton, B. W., & Skrutskie, M. F. 1996, Proc. SPIE, 2863, 2
Monnier, J. D., Tuthill, P. G., & Danchi, W. C. 1999, ApJL, 525, L97
Monnier, J. D., Zhao, M., Pedretti, E., et al. 2011, ApJL, 742, L1
Mora, M. D., Larsen, S. S., Kissler-Patig, M., Brodie, J. P., & Richtler, T. 2009, yCat, 350, 10
Nasa, & Heasarc 2018, yCat, 1020, 39
Ney, E. P., & Merrill, K. M. 1980, Study of Sources in AFGL Rocket Infrared Study. Tech. Rep., MA AFGL-TR-80-0050
Nowotny, W., Kerschbaum, F., Olofsson, H., & Schwarz, H. E. 2003, A&A, 403, 93
Page, M. J., Yershov, V., Breeveld, A., et al. 2014, in Proc. Swift: 10 Years of Discovery (SWIFT 10), ed. P. Caraveo et al. (Trieste: PoS), 37
Price, S. D., & Murdock, T. L. 1983, AFGL, 161, 0
Riebel, D., Meixner, M., Fraser, O., et al. 2010, ApJ, 723, 1195
Riebel, D., Srinivasan, S., Sargent, B., & Meixner, M. 2012, ApJ, 753, 71
Riebel, D., Boyer, M. L., Srinivasan, S., et al., et al. 2015, ApJ, 807, 1
Ryon, J. E., Bastian, N., Adamo, A., et al., et al. 2015, MNRAS, 452, 525
Samus, N. N., Kazarovets, E. V., Durlevich, O. V., Kireeva, N. N., & Pastukhova, E. N. 2017, ARep, 61, 80
Sandage, A. 1971, ApJ, 166, 13

Scargle, J. D. 1982, ApJ, 263, 835
Siess, L. 2007, A&A, 476, 893
Silva-Villa, E., & Larsen, S. S. 2011, A&A, 529, A25
Soszyński, I., Udalski, A., Szymański, M. K., et al. 2009, AcA, 59, 239
Soszyński, I., Udalski, A., Szymański, M. K., et al. 2011, AcA, 61, 217
Soulain, A., Millour, F., Lopez, B., et al. 2018, A&A, 618, A108
Stetson, P. B. 1987, PASP, 99, 191
Taranova, O. G., & Shenavrin, V. I. 2011, AstL, 37, 30
Thompson, T. A., Prieto, J. L., Stanek, K. Z., et al. 2009, ApJ, 705, 1364
Thorne, K. S., & Zytkow, A. N. 1975, ApJL, 199, L19
Tully, R. B., Courtois, H. M., & Sorce, J. G. 2017, yCat, 50, 0
Tuthill, P. G., Monnier, J. D., & Danchi, W. C. 1999, Natur, 398, 487
Udalski, A., Szymanski, M., Kaluzny, J., et al. 1993, AcA, 43, 289
Usov, V. V. 1991, MNRAS, 252, 49
Vanderplas, J. 2015, gatspy: General tools for Astronomical Time Series in Python, Zenodo, doi:10.5281/zenodo.14833)
VanderPlas, J. T., & Ivezić, Ž. 2015, ApJ, 812, 18
Vijh, U. P., Meixner, M., Babler, B., et al. 2009, AJ, 137, 3139
Vucetic, M. M., Arbutina, B., & Urosevic, D. 2015, yCat, 744, 609
Werner, M. W., Roellig, T. L., Low, F. J., et al., et al. 2004, ApJS, 154, 1
Whitelock, P. A., Feast, M. W., Marang, F., & Breedt, E. 2004, MNRAS, 352, 447
Whitelock, P. A., Kasliwal, M., & Boyer, M. 2017, in Wide-Field Variability Surveys: A 21st Century Perspective, Vol. 152, ed. M. Catelan & W. Gieren (Les Ulis: EDP Sciences), 01009
Whitelock, P. A., Menzies, J. W., Feast, M. W., & Marigo, P. 2018, MNRAS, 473, 173
Whitelock, P. A., Menzies, J. W., Feast, M. W., Nsengiyumva, F., & Matsunaga, N. 2013, MNRAS, 428, 2216
Williams, P. M. 2014, MNRAS, 445, 1253
Williams, P. M., Cohen, M., van der Hucht, K. A., Bouchet, P., & Vacca, W. D. 1995, MNRAS, 275, 889
Williams, P. M., van der Hucht, K. A., Pollock, A. M. T., et al. 1990, MNRAS, 243, 662
Williams, P. M., van der Hucht, K. A., & The, P. S. 1987, A&A, 182, 91
Williams, P. M., van der Hucht, K. A., van Wyk, F., et al. 2012, MNRAS, 420, 2526
Williams, P. M., Marchenko, S. V., Marston, A. P., et al. 2009, MNRAS, 395, 1749
Winkler, P. F., Blair, W. P., & Long, K. S. 2017, ApJ, 839, 83
Wood, P. R., Alcock, C., Allsman, R. A., et al. 1999, in IAU Symp. 191, Asymptotic Giant Branch Stars, ed. T. Le Bertre, A. Lebre, & C. Waelkens (San Francisco, CA: ASP), 151
Wright, E. L., Eisenhardt, P. R. M., Mainzer, A. K., et al. 2010, AJ, 140, 1868